Faculty of Engineering

Cornering CFD Simulation

Final Research Report submitted for EGH400-2 Semester 2 2022

Student Name:	[Jacob, Garcia-Pavy]
Supervisor:	[Dr. David Holmes, Professor in Mechanical Design & Manufacturing]
Submission Date:	[28th October 2022]

Gmail

Jacob gp <jacobgp99@gmail.com>

We've processed your Assignment extension request FORM-AEX-273502

no-reply@qut.edu.au <no-reply@qut.edu.au> Tue, Oct 25, 2022 at 3:15 PM
To: jacob.garciapavy@connect.qut.edu.au

Hi Jacob,

Thank you for your assignment extension request **(FORM-AEX-273502)**.

We have approved your request and the due date for your assignment **Final Project Report**, for unit EGH400-2 has been extended by 48 hours from the original due date. If your unit outline does not specify that your assignment is eligible for an extension, this confirmation email is not valid and unless you submit by the original due date, the late assessment policy will apply.

You are responsible for ensuring that this assignment is eligible for extension before submitting it after the original due date. Check your unit outline for eligibility.

Be aware that a copy of this email is kept on file. You should not alter this email in any way. Email notifications that have been altered or differ in any way from the original may result in an allegation of student misconduct as set out in the Student Code of Conduct.

Need extra support? You can access free, confidential counselling with qualified professionals. We also offer planning and support if you have a disability, injury or health condition that affects your ability to study. If you are struggling to meet your university commitments, academic support is also available.

Have a question? You can contact us by email or phone. We're also available to help you on campus or via online chat. Visit the HiQ website for our contact details and opening hours.

Email us	+61 7 3138 2000

HiQ is your place to go for **student services, support** and **general enquiries:** qut.to/abouthiq

hi, how can we help you?

You have received this email because you have submitted an assignment extension request. View our Privacy and Security statement.

Ref ID: 10012478 FORM-AEX-273502

LIST OF KEYWORDS

QUTM, Aerodynamics, CFD, Cornering

ABBREVIATIONS & DEFINITIONS

QUTM – Queensland University of Technology Motorsport

FSAE – Formula Society of Automotive

EV4 – Electric Vehicle 4

COG – Centre of Gravity

COP – Centre of Pressure

CFD – Computational Fluid Dynamics

CR – Cornering Radius

COR – Centre of Curvature

ABSTRACT

The QUTM team competes in the FSAE competition which judges competitors across several static and dynamic events. The competition places a strong emphasis on cornering performance and related design justification. Aerodynamics plays a critical role in vehicle performance, with evident benefits towards cornering abilities demonstrated through downforce. However, cornering conditions introduce variable airflow velocity and curvature, and thus requires special accommodation and analysis. The condition is strictly limited to numerical work due to limitations regarding experimental replication. Therefore, this report aims to develop a *Computational Fluid Dynamic* method with high levels of confidence to simulate aerodynamics in cornering conditions for the QUTM team.

With the inability of experimental validation, the proposed methodology aimed to capture high levels of confidence by replicating Keough's numerical case study on "*the cornering effects on the Ahmed body*". The simulation deployed *K-e Realizable* an effective and efficient mathematical model under the Moving Reference Frame approach. This stage concluded appropriate aerodynamic characteristics of the Ahmed body in conjunction with translational results concluded by Hughes, and rotational results reported by Keough.

The project concluded simulations on the aerodynamic elements of the EV including its: front wing, wheels, chassis, undertray, side wings and rear wing. The simulations displayed linear fluid velocity, and relative curvature congruent of cornering conditions. The results concluded common cornering characteristics documented amongst the literature with asymmetry exhibited in pressure distribution and the trailing wake of the element with strengthened features on the outboard sides. The project was able to conclude the appropriate aerodynamic differences between translational and rotational motion regarding the front wing. Variable airflow increased drag and side force, along with moments including yaw, pitch, and roll, with a significance decrease in downforce. *EV* simulations exhibited common cornering characteristics but could not specify absolute confidence due to a lack of verification with translational motion. The numerical method offers significant development and resources for the QUTM team towards cornering aerodynamics which can facilitate success in the FSAE competition.

TABLE OF CONTENTS

LIST OF FIGURES

LIST OF TABLES

STATEMENT OF ORIGINAL AUTHORSHIP

To the best of my knowledge the report does not contain material previously published or written except where reference is made. All concluded results were undertaken by myself, providing unique resources and development for the QUTM team.

1.0 INTRODUCTION

QUT Motorsport is a student-run faculty which designs, engineers, builds and markets a single seat electric vehicle for the *FSAE-Australasia* competition. *FSAE* is an international student design competition which separately evaluates combustion and electric small Formula vehicles across several static and dynamic events. The former (titled *Cost*, *Presentation* and *Design*) judges the vehicle's design justification, presentation and cost. Whilst the latter (*Acceleration*, *Skid-Pad*, *Autocross*, *Fuel Economy* & *Endurance*) evaluates on-track performance. The competition heavily focuses on cornering abilities being explicitly demonstrated in the *Skid-Pad* event which times competitors under constant cornering conditions (Appendix A). Hence, competitors, including *QUTM* and the current *EV* displayed in figure 1 has a critical interest and underlying design parameter surrounding cornering performance.

Figure 1: EV [1]

1.1 BACKGROUND

Cornering exhibits a non-inertial frame of reference satisfied through two 'fictious forces', centripetal and centrifugal. Centripetal force acts on the cornering vehicle perpendicular towards its Centre of Radius (COR). The centripetal eq.1 is the vehicle's lateral cornering force related to its mass, velocity, and Cornering Radius (CR). This lateral cornering force is sustained and often limited by the vehicle's frictional grip between its tyres and the road (eq.2). Ultimately, cornering performance is governed by the vehicle's frictional component which is significantly influenced by mechanics and aerodynamics.

$$F_{Centripetal} = \frac{mv^2}{r} \dots (1), \qquad F_{friction} = \mu_S N \dots (2)$$

Mechanics and aerodynamics are significantly intertwined in vehicle performance. Mechanics with regards to cornering considers: the inertial moments (yaw, pitch and roll) induced by the reciprocating centrifugal forces; cornering behaviour (oversteer/understeer) based on the vehicle's Centre of Gravity (COG); and tyre deformation (slip-angle). Mechanical performance offers limited optimisation towards cornering performance in comparison to aerodynamics.

1.1 AERODYNAMICS

External aerodynamics studies an object's motion through fluid which becomes increasingly apparent surrounding high-performance vehicles, with the effects being proportional to velocity squared. An object travelling through fluid experiences lift, drag and side forces on its respective surfaces, with collective forces acting on the body considered about the Centre of Pressure (COP). Aerodynamics influences cornering mechanics and behaviour by affecting moments and shifting the vehicle's COG. However, its most prominent effect is the generation of negative lift. Downforce can greatly enhance cornering abilities, increasing normal load and available frictional grip ('aerodynamic grip') with no added 'mass' (eq.1).

The EV features several downforce elements including its front and rear wing. The specific design utilises 'inverted aerofoils' channelled with side plates to redirect fluid-flow. Downforce is created due to the stagnation and acceleration of fluid velocity over the element's upper and lower surfaces. Bernoulli (eq.3) illustrates the inversed relationship between velocity and pressure. Pressure is associated with a force which acts on the respective surfaces. The upper surface experiences a negative lift force which overwhelms the positive under-side. Consequently, the wing's design and lift are the most significant parameters regarding cornering performance but are closely formulated with drag.

$$P_1 - P_2 = \frac{1}{2}\rho v_2^2 - \frac{1}{2}\rho v_1^2 \dots (3)$$

Drag is the aerodynamic resistance of the object's motion which consists of different forms. Friction drag occurs due to the adhering of fluid particles over the surface developing a thin boundary layer of viscous fluid. The flowing particles above the layer are consequently slowed by the non-moving particles resulting in skin friction. Whilst pressure and form are closely related to fluid displacement and pressure, with the latter in respects to fluid separation. Vehicular drag is significantly attributed to pressure drag associated with fluid separation of the vehicle's trailing wake. Overall, aerodynamics is critical to vehicle performance, especially cornering conditions.

1.1.1 CORNERING AIRFLOW

Cornering airflow is inherently different to translational motion. Intuitively, the airflow follows that of the vehicle's path depicted in figure 2. The vehicle can be considered with constant angular velocity about a fixed-point representative of constant radius and cornering condition. The vehicle experiences differing fluid velocity with distance from the COR. Airflow curvature, named yaw angle (φ) differs across the vehicle with displacement from the COR. Further supplementary cornering equations are contained in Appendix B. Cornering aerodynamics is significantly different to translational motion and thus, requires specific analysis in the respective condition.

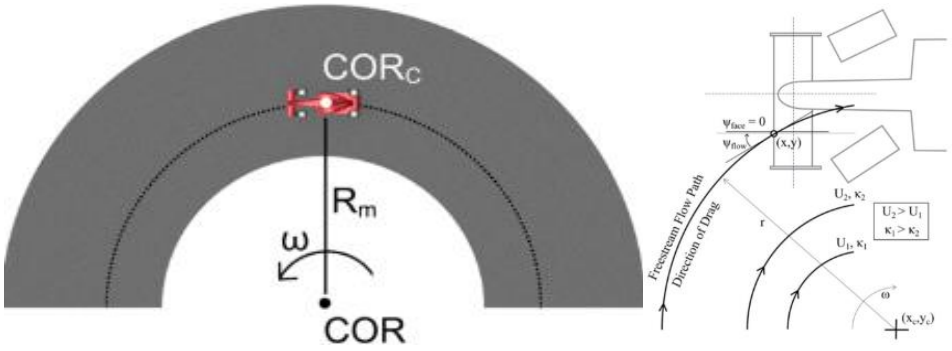

Figure 2: Cornering Airflow [2]

1.2 CONTEXT

Aerodynamics is a critical interest of *QUTM* and the *EV*. *QUTM* has dedicated significant effort and development towards numerical and experimental work to optimise and validate the *EV*'s aero package for the *FSAE* competition. Aerodynamic downforce evidently benefits cornering performance with apparent differences to translational motion. There have been two prior thesis projects conducted by *Ben Charter & William Smitheram* who explored cornering aerodynamics on several aerodynamic elements and a simplified *EV*. However, the condition is yet to be concluded and implemented for *QUTM*.

1.3 PURPOSE

This thesis aims to conclude a numerical cornering simulation dedicated for the *QUT Motorsport* team's Formula Student Vehicle, the *EV4*. The results hope to facilitate future improvement within the FSAE competition allowing the team to optimise and justify the *EV4*'s aero package. The project has several objectives which must be concluded to ensure project success with high levels of:

- Confidence
- Usability
- Appropriateness

1.4 Significance, Scope and Definition

The project's scope and significance will be limited to steady-state conditions. The project aims to secure a *Computational Fluid Dynamic* (CFD) simulation with high levels of confidence and possible simplification on the physical geometry to enhance its usability for the *QUTM* team. The project does not intend to conduct performance optimisation but will report and verify the unique differences of cornering aerodynamics. The thesis project exerts several research questions regarding: (1) Experimental Testing; (2) Numerical Limitations; (3) Cornering Numerical Simulations; (4) FSAE's Vehicles Aerodynamics.

2.0 LITERATURE REVIEW

2.1 EXPERIMENTAL TESTING

Cornering aerodynamics has proven difficult to experimentally replicate. Experimental techniques including whirling arms, rotary rigs, curved test sections and bent models replicate certain aspects of cornering conditions but are all compromised [3]. Keough et al [4] has developed an experimental apparatus capable of continuous curved airflow but remains in its infancy. Currently the condition can only be experimentally replicated through on-track/road testing which contains significant variability.

The consecutive experimental and numerical reports conducted by Tsubokura et al [5] and Okada et al [6] investigated two medium-sized sedans in meandering motion. The numerical report offers significant development surrounding cornering and cross-transient wind simulations. Whilst the experimental component noted difficulties gaining meaningful results from the driving vehicle, basing all-on road forces on the integration of the surface pressure measurements calibrated with wind-tunnel testing of yaw angle [7]. Strictly yaw is not a complete representation of cornering conditions [8]. However, wind-tunnel testing on elements under yaw and a rolling road is currently the most effective method [8]. Consequently, cornering aerodynamics has heavily relied on numerical work which presents limitations regarding validity.

2.2 NUMERICAL SIMULATIONS

Computational Fluid Dynamic (CFD) simulations has gain significant popularity amongst aerodynamicists utilising the *Finite Volume Method* (FVM). However, the ability of numerical work to yield meaningful results depends on two factors: the validity of the physical and mathematical models for the prescribed flow phenomena; and the accuracy of the approximations of the equations pertaining the mathematical model [9]. Vehicular aerodynamics is highly turbulent with significant flow separation and associated Reynolds number (Re) [10]. A *Direct Numerical Simulation* (DNS) is not possible requiring an exceeding mesh resolution and computational power to resolve the Kolmogorov scale [9]. Thus, respective simulations are limited to either numerical approximations: *Reynolds Averaged Navier-Stokes* (RANS) or *Large Eddy Simulations* (LES) [9,10]. Numerical work displays concerns regarding computational power and accuracy with the inability of experimental validation. Toet [8] suggests the importance of numerical confidence through either validation/correlation with translational motion, yaw testing or on-track performance. Whilst the physical model including its geometric discretisation is a major component towards computational validity.

2.2.1 MESH

FVM discretises the geometric domain into an arbitrary mesh of non-overlapping elements (finite volumes). The quality of the mesh and connectivity plays a vital role in the accuracy and stability of the numerical computation [11]. In which conversation fluxes and terms are discretised through each

element and its neighbour [12]. Notably, polyhedral elements increase flexibility and robustness in the meshing of geometrically complex domains and can lead to higher quality solutions [13]. Mesh quality must be assessed through parameters such as aspect ratio and orthogonal quality [11]. Whilst dimensionless properties such as $x^+, y^+ \, and \, z^+$ give an indication of the required streamwise and spanwise resolution. Piomelli [14] recommends a first cell height at the wall of $y^+ < 1$, and a streamwise and spanwise resolution of respectively $\Delta x^+ = 50 - 150, \Delta z^+ = 15 - 40$. Whilst it is generally appropriate to utilise a y^+ near wall value of 30, with the respective formulation contained in Appendix C [15]. Overall, numerical results lack validity, and must deploy appropriate meshing and numerical methods to successfully deploy the cornering condition.

2.3 CORNERING NUMERICAL WORK

The cornering condition requires consideration of both the topology of the computational domain, and the simulation of motion. Numerous case studies have proven the effectiveness of both the curved and rectangular domain illustrated in figure 3 [7, 16, 17, 18, 19, 20,21]. The construction of the curved domain is much simpler but is limited to a specific cornering radius [7]. Whilst the construction of the rectangular domain with various 'inlets' and 'outlets' allow a multitude of cornering radii and fluid physics permitting translational and dynamic motion [7, 17]. The rectangular domain is heavily favoured amongst aerodynamicists deployed through an array of numerical methods.

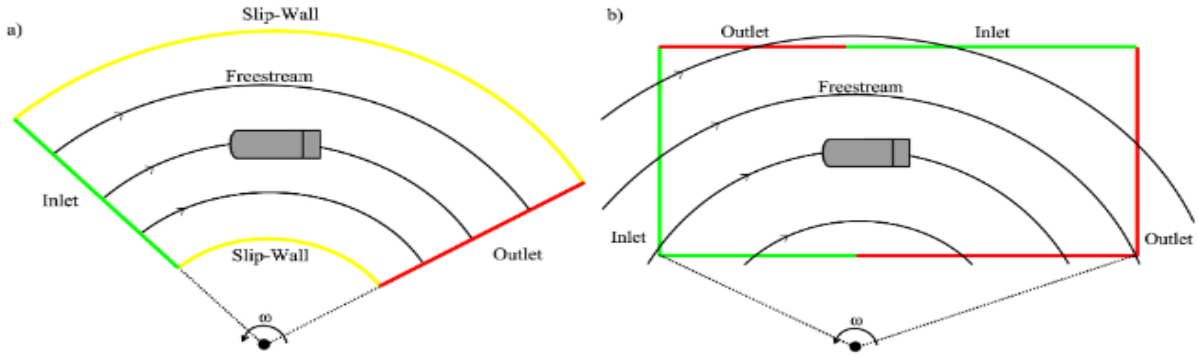

Figure 3: The Curved and Rectangular Domain [3]

The literature displays several applicable rotational methods including: the *Moving Reference Frame* (MRF), *Rigid Body Motion* (RBM) and the *Overset Mesh* [17]. The overset method permits complex combinations of motion with additional computational cost and complexity [17]. The RBM technique calculates the grid flux based on prescribed displacement of the entire mesh at each time-step [17]. This method is an alternative to the overset mesh which avoids its associated interpolation errors [17]. The MRF approach simulates motion through additional grid flux term to the conservation equations upon a stationary mesh [17]. Patel et al [17] advises against the use within unsteady flow solutions. However, the literature heavily promotes the utilisation and effectiveness of MRF, most prolifically documented by case studies conducted by Keough et al [7]. With that said, all numerical studies display

similar approaches to accommodate the unique fluid condition and alterations towards aerodynamic calculations.

Rotational motion requires certain accommodation to correctly account for the change in aerodynamic motion. The linear drag formulation is inadequate with drag resisting the curved motion of the object [7]. Drag becomes proportional to the moment acting on the body in the same circular path [7]. Side force varies but remains orthogonal to drag [7]. Patel et al [17] provides CFD implementation to compute the adopted drag and side force equations given by Joseffson et al [18] contained in Appendix B. Lift remains vertical but does alter due to vehicle roll [17]. Whilst the relative Re across the vehicle was proven insignificant by Keough et al [3]. All case studies utilise a non-inertial reference frame along with relative velocity and deceleration terms to accommodate for the cornering flow behaviour.

2.3.1 Patel et al [17] & Keough et al [19] Case Studies

Patel et al [17] and Keough et al [19] case studies numerically explored cornering aerodynamics of an inverted wing in ground effect. The work distinctively compares the aerodynamic differences between straight-line, fix yaw and cornering conditions. In addition, the papers illustrate what can be achieved regarding yaw wind-tunnel testing in representing true cornering conditions.

Patel et al [17] utilised the rectangular domain under RBM. The numerical case study deployed *Detached Eddy Simulation* (DES) which combines the respective advantages of RANS and LES regarding attached and unsteady flow [22]. The numerical method exerted high levels of confidence through 'validation simulations' of translational motion with corresponding experimental testing. Keough et al [19] utilised the rectangular domain under MRF in steady state, deployed through *K-e Realizable* which has been proven inferior but effective requiring a small fraction of the computational resources [23]. The case studies utilised a rolling road with velocity-inlets set to 0m/s where rotation was prescribed through differing method. Despite the apparent differences and associated quality, the results closely coincided.

The fixed yaw and cornering condition displayed generalised similarity due to its asymmetric fluid-field. Downforce concluded from translational motion decreased by .4% and .5% in cornering and fixed yaw conditions [17]. The cornering and yaw conditions increased drag by 5% and 1%. However, there were notable discrepancies between the respective conditions which prompts caution of yaw experiments. The downstream trajectory of the vortex system significantly altered which strengthened the laterally induced vortexes most prominently in cornering conditions [17]. The case study suggests flexibility regarding numerical methods, and yaw wind-tunnel with representative data concerning cornering aerodynamics

2.3.2 Keough et al [7] Case Study

Keough et al [7] numerical case study, *the "aerodynamic effects on a cornering Ahmed body"* provides valuable development towards numerical cornering simulations. The case study appropriates high levels of confidence through validation of its numerical methodology with translational Ahmed body wind-tunnel testing conducted by Leinhart and Becker [24]. The 'validation simulations' displayed favourable agreement, accurately capturing its time-average wake deficit and dissipation, however, inflated aerodynamic forces due to a high blockage ratio and associated constraining effect [7].

Vehicular aerodynamicists heavily favour simple bodies rather than specific vehicle geometries. This is to ensure that results are independent of geometric specificities which can allow a collaborative effort and conclusion towards common vehicular aerodynamic characteristics [7]. The Ahmed body has been heavily studied since inception and experimental work in 1984 by Ahmed et al [25]. The Ahmed body maintains flow attachment overs its frontal section allowing investigation into the most significant and common aerodynamic characteristics occurring towards a vehicle's aft [25]. The 25-degree slant angle was utilised in the case study providing optimal reattachment phenomena [26]. A generalised flow regime adopted by Keough is provided in figure 4. The Ahmed body is an extensive tool utilised by aerodynamicists to validate new experimental and numerical set-ups with significant resources.

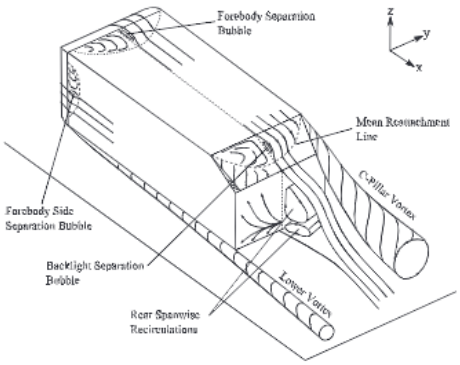

Figure 4: Ahmed Body Flow Characteristics [7]

Keough utilised the domain and geometry construction illustrated figure 5. LES was deployed due to its proven superiority allowing the identification of lower vortices and an accurate three-dimensional understanding of the flow [27]. Time was nondimensionalised according to the time taken for a fluid particle to travel the length of the body, with a time-step of 1e-04 ensuring a .95 CFL number and appropriate median velocity magnitude with experimental locations [7]. The results concluded the significant effect on pressure distribution with variable fluid velocity and angle. The outboard C-pillar was significantly strengthened and weakened on the inboard side. The inboard side observed an extension of a separation bubble resulting in gentler downwash [7]. The case study concluded that increased curvature of the vehicle's path linearly increased drag, yawing moment and side force with a

decrease in lift. Overall, Keough's numerical case studies offer significant development towards cornering simulations with high levels of confidence.

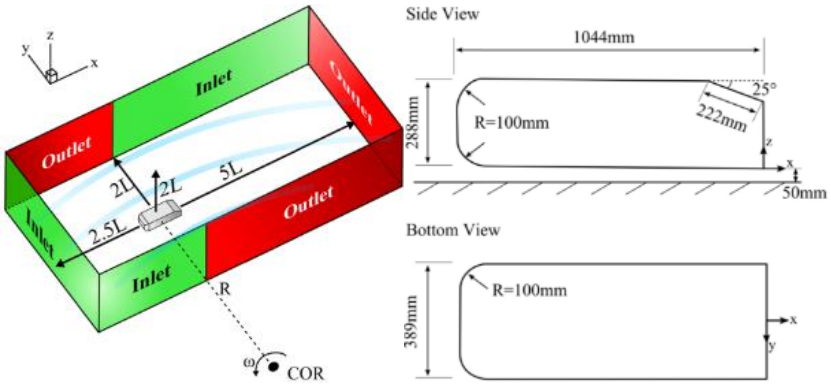

Figure 5: Domain and Geometry Construction [7]

2.4 FSAE INVESTIGATIONS

Aerodynamics is a critical interest amongst FSAE teams. The literature offers several experimental and numerical case studies in translational conditions. Further assistance is offered through LEAP with video tutorials dedicated on CFD FSAE simulations [28]. Although the results are geometry dependent, the numerical case studies conducted by Ockerby et al [15], Oxyzoglou et al [29] and Dharmawan et al [30] displayed minor discrepancies between aerodynamic characteristics and forces. Furthermore, the rectangular domain permits analysis of translational condition, hence, can corroborate with the FSAE literature to further confidence. Overall, the FSAE literatures provides valuable results and information applicable for FSAE cornering simulations.

2.5 Summary

Cornering aerodynamics has heavily relied on numerical work due to the associated limitations of experimental replication. With that said, numerical work pertains differing limitations surrounding computational power and accuracy. The literature displays substantial flexibility to accommodate for the cornering condition. However, most efforts have been dedicated towards the efficient rectangular domain and MRF method. Keough's case study "the *aerodynamic effects on a cornering Ahmed body"* exhibits high levels of confidence in its numerical method due to its ability to simulate a multitude of fluid conditions. The Ahmed body has been heavily documented in translational motion allowing subsequent validation of the numerical method set in translational motion. Furthermore, confidence in the cornering condition can be provided through correlation with yaw wind-tunnel and on-board track testing. Overall, the literature provides significant resources towards numerical development of a cornering simulation on a *FSAE* vehicle.

3.0 METHODOLOGY

This project aims to secure a CFD cornering simulation for the *EV4* with high levels of confidence, practicality and usability for the *QUTM* team. The validity of the numerical method is of critical concern due to numerical limitations and the inability of experimental validation. There is potential future work regarding experimental yaw-testing utilising QUT's small scale wind-tunnel and on-track testing which could be utilised to correlate with/against the numerical results. However, the project will be limited to numerical work asserting high levels of confidence through successive stages towards the EV4 highlighted in figure 5.

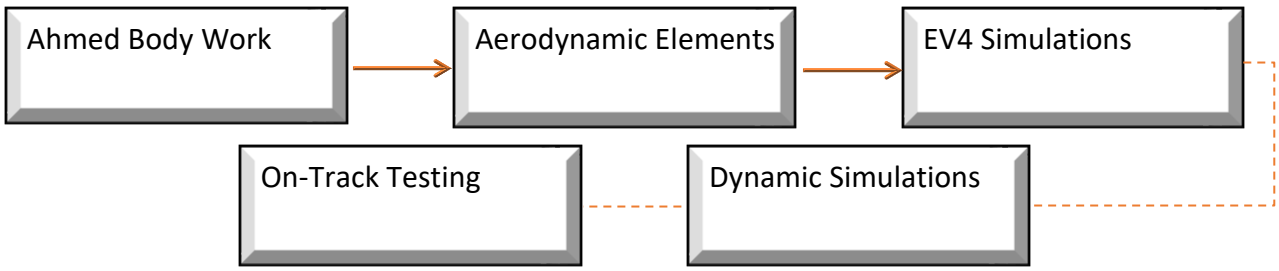

Figure 6: Methodology Figure

3.1 Ahmed Body Verification

Keough et al [7] case study '*aerodynamic effects on a cornering Ahmed body*' deploys high levels of confidence in its numerical method through 'translational validation simulations' utilising empirical results concluded by Leinhart and Becker [24]. The project aims to exert similar levels of confidence. The first stage aims to replicate the numerical method and results documented by Keough. A notable limitation pertaining this stage is computational power and time. Complete replication of the respective mesh count of 50 million elements, under the superior and computationally demanding LES model with a given time-step of 1e-04 is unfeasible, and limits efforts and time towards the successive stages.

This stage and consecutive simulations will utilise *K-e Realizable*, an effective and efficient alternative proven by Keough et al [19]. Keough's methodology will be followed: with simulations on a Cornering Radius of 0 (translational), 5 and 20L under a tangential velocity of 25m/s; the domain and geometry illustrated in figure 5 will be reconstructed; whilst the MRF approach will be deployed with an absolute velocity-inlet of 0m/s; residuals will be set to 1e-06 at 1500 iterations. Simulations will utilise the computational power of the High-Performance-Computer (HPC) available to research students at QUT to improve quality and efficiency, allowing more representative results. Simulations will be set in steady-state and seek further corroboration of the noted inferior depiction of the trailing wake with Hughes [26] numerical *K-e Realizable* results on the Ahmed body. Overall, stage success will be determined through comparison with Keough's and Hughes' results. .

3.2 Aerodynamic Elements

Upon success and confidence in the numerical method, the aerodynamic elements will be integrated. The aerodynamic elements include the: front wing, chassis, wheels, side wings, undertray and rear wing due to its prominent affect on the EV's aerodynamics. This stage aims to build and instil greater confidence through simpler and less computationally demanding simulations towards the EV. The results will be utilised and cross-referenced for the successive simulations on the EV. All geometries will be accessed through the QUTM's PDM folder. Geometry simplification may be necessary or beneficial towards the EV simulation being most apparent to the chassis and wheels. Preliminary design work will prepare the models, removing unnecessary components, holes, duplicate faces, split edges and small faces. This stage aims to conclude the geometries, domain and meshing strategy for the EV simulation, whilst reducing computational time and allowing comparability between results. All simulations will utilise a cornering radius of 0 and 5 metres under a tangential velocity of 16.67m/s to illustrate the prominent effects of cornering conditions.

3.3 EV Simulation

The EV4 will utilise the concluded geometries, domain and meshing strategy from the *aerodynamic element stage* under the same fluid conditions set to a cornering radius of 0 and 5 metres with a tangential velocity of 16.67m/s. Rotating wheels will be deployed following the same methodology utilised for the wheel simulations in the *aerodynamic element stage*. To verify confidence within the numerical simulation, careful analysis will be undertaken between the previous stage regarding intended aerodynamic forces, moments and characteristics of the aerodynamic elements with consideration of the intended upstream and downstream effect. The front wing and nose cone make initial fluid contact being relatively unaffected by the downstream flow, and hence share the greatest similarity between the stages.

4.0 RESULTS

4.1 Ahmed Body Verification

Keough's numerical case study was replicated under certain accommodations regarding computational resources and time. This stage deployed Keough's numerical method, geometry and domain construction. However, could not fulfil the aspired quality associated with the mesh size and mathematical model. It must be noted that the mesh refinement test contained in Appendix D prompts further refinement due to large force discrepancies with the prior mesh iteration. However, the results conducted on 'mesh 2' concluded sufficient validation allowing confidence in the numerical method.

The simulations displayed accurate representation of cornering fluid-flow observed through the velocity contour-lines figures 7, 8 and 9 respectively for a 0, 5 and 20L cornering radius. The figures display the intended velocity gradient and curvature of fluid-flow for the respective fluid conditions. Whilst closely coinciding with Keough's figures presented on the right displaying the asymmetrical trailing wake and strengthened outboard C-pillar vortex in cornering conditions.

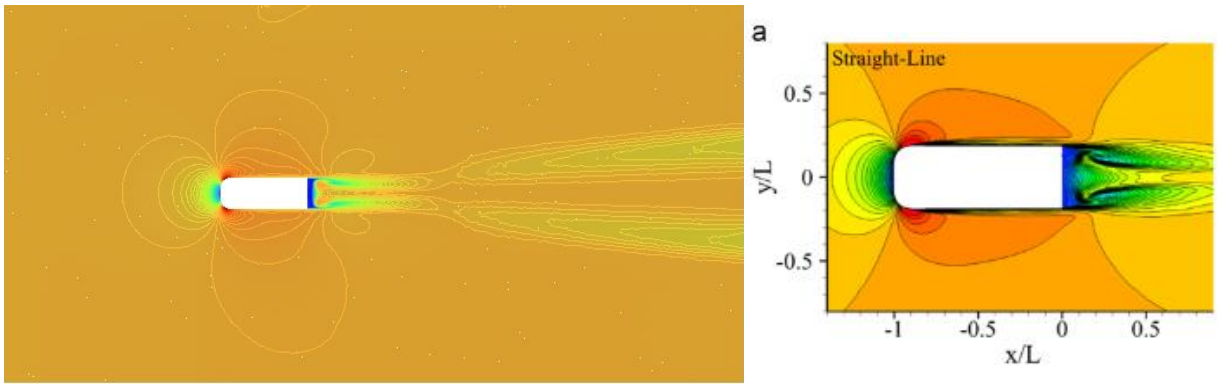

Figure 7: Translational Velocity Contour Comparison with Keough (right)

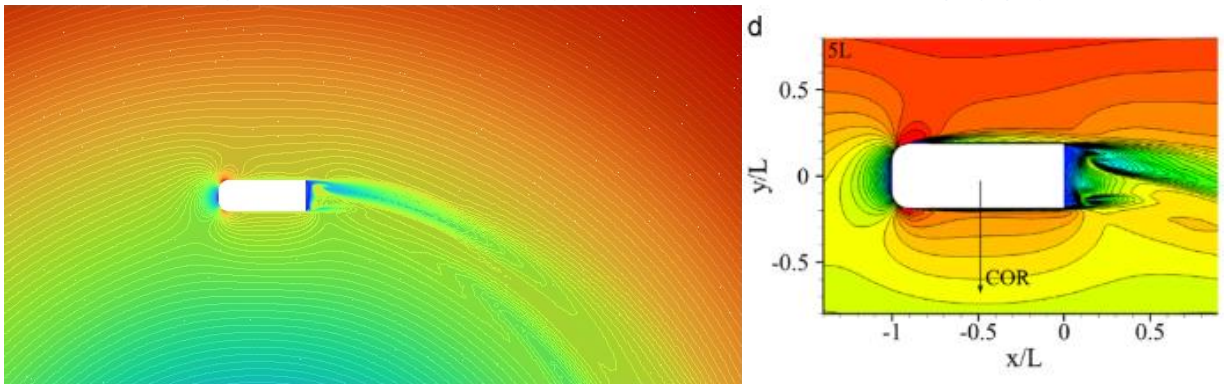

Figure 8: 5L Cornering Radius Velocity Contour Comparison with Keough (right)

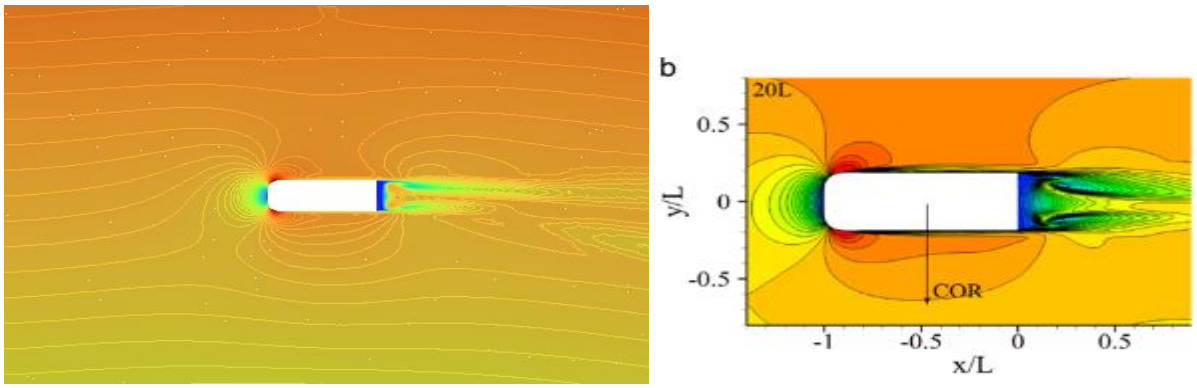

Figure 9: 20L Cornering Radius Velocity Contour Comparison with Keough (right)

Appendix E contains further results and figures regarding pressure, pressure-coefficients, side-plane velocity and trailing wake contours (taken from x=.522, .599 and 1.02). All results display direct comparison to Keough with minor discrepancies pertaining the trailing wake. The trailing wake lacks quality in comparison to Keough's depiction illustrated in Appendix F. Most importantly the results acknowledge the inferior nature of *K-e Realizable* with limited depiction of the lower trailing vortexes. However, a representative numerical simulation with *K-e Realizable* undertaken by Hughes infers high levels of confidence with close resemblance of recirculating vortexes displayed in the side and trailing wake contours illustrated in Appendix E and F.

Notably the stage falls short in replicating Keough's aerodynamic forces. Table 2 concluded correct yaw, and side force coefficients, along with the intended increase in yaw, drag and side force with increased curvature. However, the results display large discrepancy in its calculated drag and lift coefficients against Keough, and its previous mesh iteration. Overall, the stage concluded appropriate replication of the numerical method with sufficient confidence but highlights concern regarding LES and mesh refinement.

Simulation	Cd		Cl		Cy		Cs	
	Sim	Keough	Sim	Keough	Sim	Keough	Sim	Keough
0m	0.245	.324	.32	.288	-0.0014	0	-0.002	0
5L	.291	.38	.315	.276	-.062	-.064	-.114	-.116
20L	.247	.32	.315	.28	-.016	-.016	-.026	-.026

Table 1: Aerodynamic Forces

4.2 Aerodynamic Elements

The aerodynamic elements were simulated utilising the numerical method for a cornering radius of 0 and 5 metres under a tangential velocity of 16.67m/s. A domain and mesh refinement test was undertaken contained in Appendix G to conclude an appropriate domain and mesh strategy which will be utilised throughout aerodynamic elements and EV simulations.

The domain test was conducted on the front wing being the first element to make initial fluid contact. Initial work extended the leading and trailing length given by Keough of 2.5L and 5.5L to Ockerby's 4L and 9L which allowed greater encapsulation of the lengthen trailing wake. The test illustrated insignificant effects between a blockage ratio of 1-3%. Whilst notably greater and lesser blockage ratios displayed significant differences in aerodynamic forces with a proportionally large effect on computational time. The concluded domain strategy will utilise the efficiency of a 3% blockage ratio, constructed around the geometry's height-width ratio with a leading and trailing length of 4L and 9L.

The mesh refinement test consisted of 4 mesh iterations. Mesh 1-3 iteratively refined areas of interest utilising body-of-influences: near-field and the trailing wake. Mesh 4 displayed the greatest reduction in downforce through domain volume refinement. Each iteration significantly increased computational time with no significant correlation to aerodynamic forces. Consequently, the mesh strategy will deploy the refinement of mesh 1 illustrated in figure 10 and discussed in Appendix G.

4.2.1 Front Wing

Simulations	Drag (N)	Lift (N)	Side Force (N)	Yaw (Nm)	Roll (Nm)	Pitch (Nm)
0m	73.529	-264.771	-0.195	0.281	0.117	295.949
5m	68.776	-309.850	-28.701	-38.137	-18.392	346.677
Verification Simulation	67.093	-342.045	19.2309	NA	NA	NA

Table 2: Translational Verification, 0 and 5 metre Aerodynamic Forces

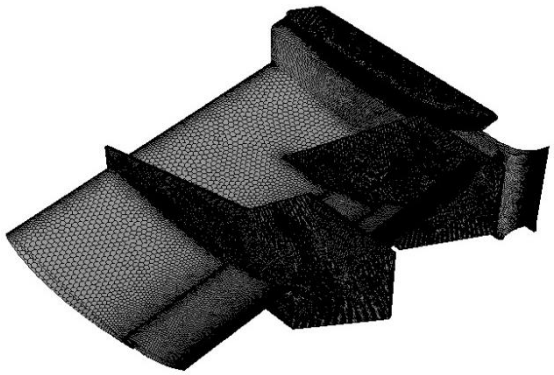

Figure 10: Front Wing Mesh

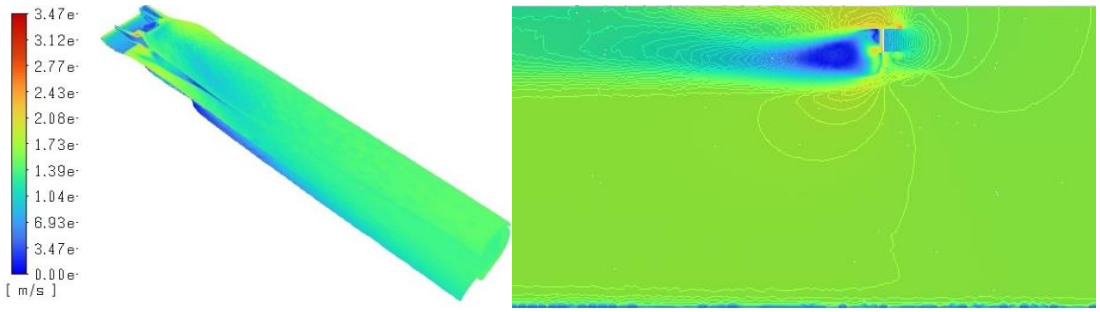

Figure 11: Translational Motion Pathlines and Velocity Contour taken at y=.25

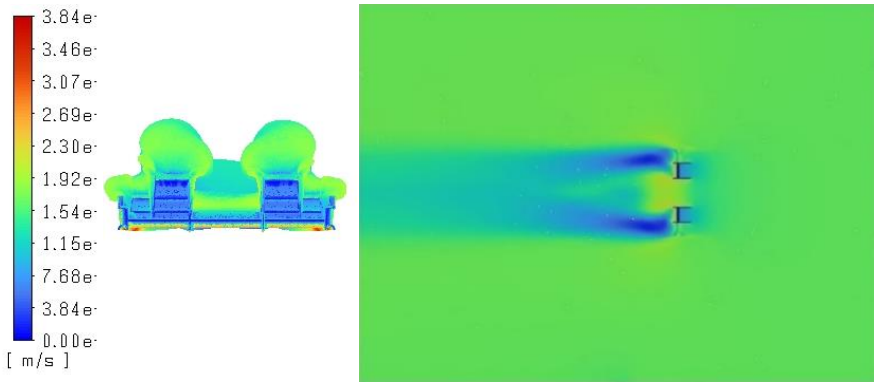

Figure 12: 0m Cornering Radius Pathlines and Velocity Contour taken at y=.25

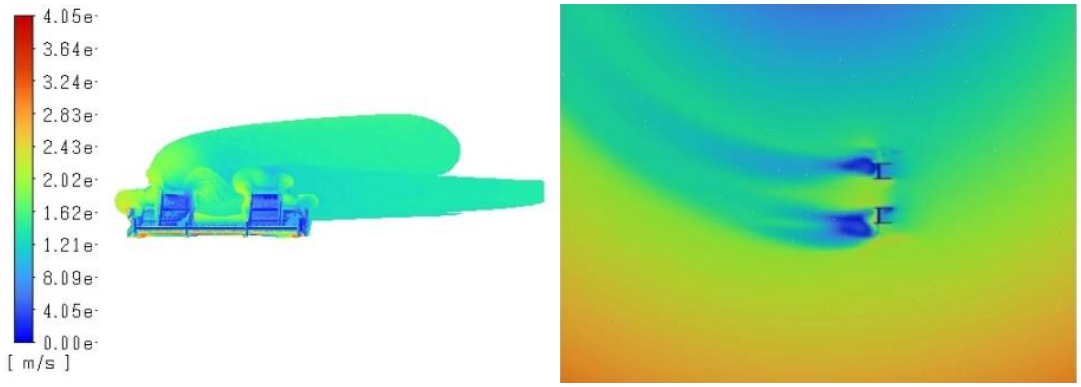

Figure 13: 5m Cornering Radius Pathlines and Velocity Contour taken at y=.25

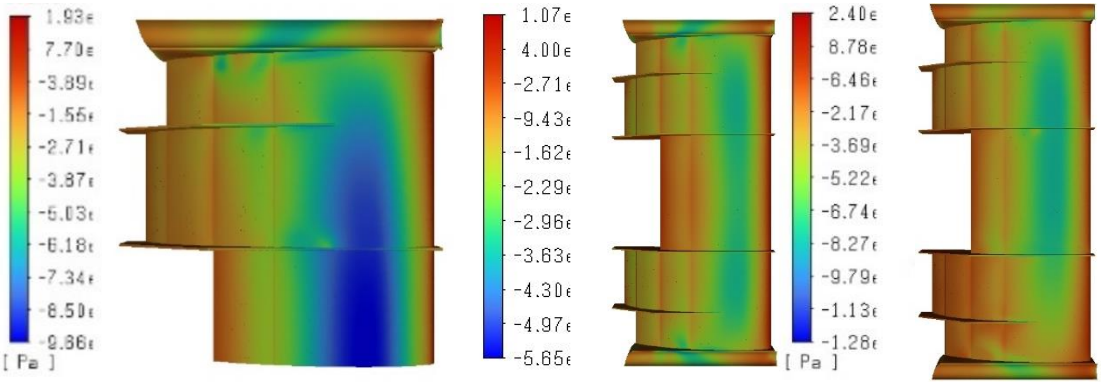

Figure 14: Pressure Distribution in Translational, 0m and 5m Cornering Radius

4.2.2 Aerodynamic Elements at a 5m Cornering Radius

5m CR	Drag (N)	Lift (N)	Side-Force (N)	Yaw (Nm)	Roll (Nm)	Pitch (Nm)
Front Wing	68.776	-309.850	-28.701	-38.137	-18.392	346.677
Undertray	36.766	-226.168	12.228	-7.421	2.340	-100.212
Right Side Wing	3.448	-7.747	0.907	-2.375	-5.440	-4.188
Left Side Wing	1.784	-9.766	-2.387	1.003	4.243	-2.483
Replica Wheels	8.818	8.628	-3.74	-0.042	-0.712	-1.836
Simplified Wheels	5.711	8.680	1.387	-0.096	0.259	-1.043
Nose Cone	1.648	5.192	-8.378	-9.524	-2.417	-7.724
Chassis	19.619	-17.097	23.509	-10.276	4.905	-9.631
Rear Wing	178.870	-398.748	110.977	-107.971	-573.069	73.648

Table 3: Aerodynamic Element Forces

4.2.3 Discussion

Results in translational motion discovered unexpected challenges. All simulations were undertaken on the HPC with limited accessibility and a lack of a user-interface. The received 'output.logs' implied its inability in translational motion with significant backflow on 22.3% of the pressure-outlets which were not observed in cornering conditions. Furthermore, the respective aerodynamic forces illustrated in table 2 were not representative of the aerodynamic differences between the fluid conditions. Thus, a verification simulation was undertaken in 4.2.1 utilising the concluded mesh and domain strategy under conventional settings with a: velocity-inlet set to 16.67m/s; pressure-outlet set to absolute 0; symmetry plane; rolling Road.

The verification simulation closely coincided with the generated figures displayed in 4.2.1 and Appendix H. However, concluded apparent discrepancies with the numerical method in translational motion regarding aerodynamic forces. The calculated forces aligned with the *FSAE* literature and the promoted the aerodynamic differences between the fluid conditions. In addition, the *aerodynamic element stage* observed difficult convergence, with a stubborn continuity residual dropping to 1e-02. Overall, the *aerodynamic stage* outlines significant caution in translational motion which diminishes the numerical method's value and ability to exert confidence for the QUTM team.

However, the aerodynamic stage was able to conclude confidence within its cornering results illustrated in Aerodynamic Force Table 3 and contained in Appendix H-K (due to the allocated page limit). Notably

moments were taken from an arbitrary position (at 0,0,0) which is not representative of the vehicle's COG but will remain for successive simulations on the EV. The table concluded an overall increase in aerodynamic drag, side force, yaw and roll compared to translational results reported by FSAE investigations. All generated figures illustrated in Appendix H-K display the intended strengthening of the outboard vortex. There was a noted formation of increased vortex velocity for the outboard and inboard side respectively for the front and rear wing (Appendix H and K) being opposite due to inversed yaw angle. Wheel simplification demonstrated a proportionally large decrease in intended drag. The spokes featured on the replica wheel allowed fluid passage and exhibited a stronger inboard trailing wake. Overall, the stage was considered successful but concluded diminished value and ability of the numerical method.

4.3 EV

EV simulations utilised the domain and meshing strategy concluded by the *aerodynamic element stage*, highlighted in figure 14. A mesh count of 87 million polyhedral cells featured 100 cells below the required .1 minimum orthogonal quality which was deemed sufficient, representing an insignificant percentage. The finalised mesh utilised:

- Curvature: 6 degrees for the wheel fillets (which were utilised to model tyre compression, resolve small cell gaps and remove sharp edges). 9 degrees for the undertray and wheels. 12 degrees for the remaining elements.
- Proximity was utilised to resolve small faces identified on the undertray providing a minimum cell count of 3 per face.
- 10 layers of last-ratio inflation at .005m was applied to all elements achieving a near wall y+ value of 30.
- Body-of-influences targeting the near-field and wake fluid-flow were given a cell size of .01 and .05metres.

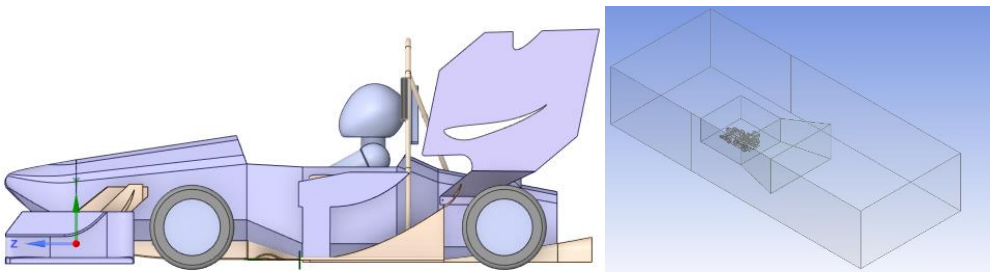

Figure 14: The EV and Domain

EV simulations were conducted on a 5-metre cornering radius with a tangential velocity of 16.67m/s. Rotating wheels were set with an angular velocity of 82 rad/s about the z-axis, specified at the respective wheel's centre measured in Space Claim (see Appendix L for related equations).

5m CR	Drag (N)	Lift (N)	Side-Force (N)	Yaw (Nm)	Roll (Nm)	Pitch (Nm)
Front Wing	39.959	-205.972	-20.990	-25.859	1.079	251.791
Undertray	12.584	-116.241	8.9638	-7.564	-8.530	-16.406
Right Side Wing	2.351	-2.474	2.893	-1.779	-2.231	-.754
Left Side Wing	5.536	-15.425	3.368	2.489	8.139	-3.178
Front Left Wheel	7.006	4.889	-2.565	3.033	-2.297	-.475
Front Right Wheel	3.449	9.829	1.471	-1.481	5.837	-4.206
Rear Left Wheel	15.100	5.241	-3.637	13.199	-2.071	9.734
Rear Right Wheel	15.629	8.379	17.485	-26.545	0.056	12.958
Nose Cone	8.589	9.020	-4.902	-5.728	0.442	-10.171
Chassis	48.368	0.500	12.278	1.462	-1.615	35.776
Rear Wing	151.651	-203.759	85.893	-76.144	23.756	-276.069
Total	310.222	-506.013	100.2578	-124.917	22.565	-1

Table 4: EV Aerodynamic Forces

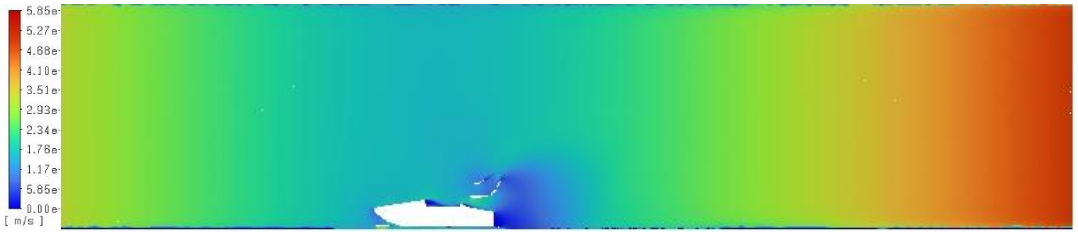

Figure 15: EV XY-Plane Velocity Contour at a 5m Cornering Radius with rotating

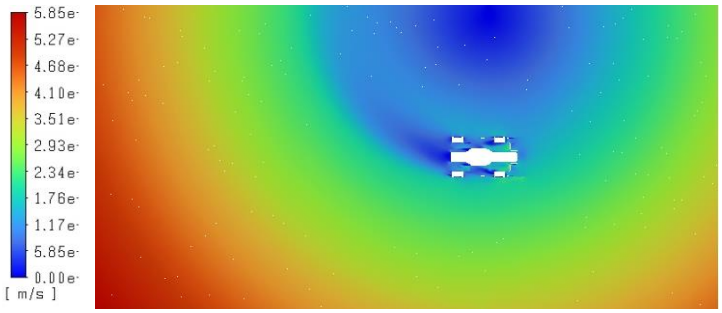

Figure 16: EV Mid-Plane Velocity Contour at a 5m Cornering Radius with rotating wheels

The concluded aerodynamic forces in table 4 display insignificant comparability with the *aerodynamic element stage*. The results display a general decrease in downforce, whilst remaining parameters were inconsistent. Although the discrepancies are largely due to the upstream and downstream effect of the elements. The front wing and nose cone which make initial fluid contact being relatively unaffected, do not coincide. In addition, results given in figures 15 and 16 display significant discrepancies with figure 17 which deployed several cornering conditions without rotating wheels at a tangential velocity of 16.67m/s. Further results including figures, aerodynamic forces and moments are contained in Appendix M and N for rolling and static wheels.

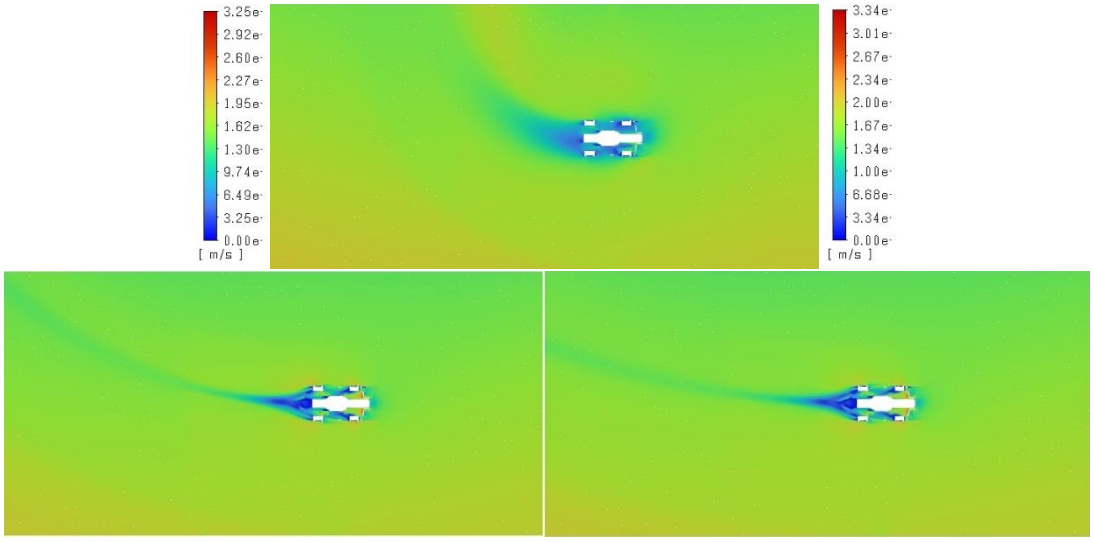

Figure 17: Midplane Velocity Contours between 5, 20 and 40 metre Cornering Radii

Currently, the numerical method does not exert high levels of confidence in EV simulations with inadequate verification. Thus, simulations were undertaken on the EV and the combined aerodynamic effect of the front wing and nose cone respectively in translational (same as verification simulation) and rotational motion. However, results could not be retrieved in time due to large queues in the HPC in week 13. Similarly, further simulations were conducted for the Skid Pad Event, and corners illustrated in the Autocross Event under the associated cornering conditions presented in Appendix L.

5.0 Conclusion

The project concluded numerical simulations on the EV and its aerodynamic elements in the cornering condition with a numerical method accessible and usable for the QUTM team presented in Appendix O. However, the project did not successfully fulfil its objective of high levels of confidence due the highlighted issues and inconsistencies. The *aerodynamic element stage* highlighted concern regarding convergence, which was unexpectedly resolved in more complex and turbulent *EV* simulations. However, *EV* simulations suffered inconsistent inflation of turbulent viscosity in its cells with a subsequent spike in residual k and e. Despite this, all reported *EV* simulations were able to resolve the issue by the 1500th iteration and obtain appropriate convergence. Overall, the numerical method was not capable of translational motion which diminishes it practicality for the QUTM team. The project concluded significant results regarding the aerodynamic elements with confidence but requires further investigation and verification through conventional translational motion simulations on the EV and cornering simulations combining the front wing and nose cone to allow high levels of confidence.

5.1 Risks

Despite the issues, the project mitigated potential risks identified in the risk assessment table contained in Appendix Q. The HPC was identified with significant severity and likelihood of inaccessibility occurring in week 13. The project would have avoided this through earlier access and simulations on the HPC. Whilst risks associated with diminishing QUTM's performance, time and efforts through unrepresentative results and confidence has been avoid through full disclosure of the numerical method's ability.

5.2 Ethics

The project addressed ethical concerns and exhibited correct engineering practices. Most importantly, all results and numerical confidence has been objectively documented with noted concerns. It is imperative the results do not mislead stakeholders, especially the QUTM team which may worsen performance and diminish iterations made by the team. The ethics table in Appendix U. displays the subsequent efforts and actions made in alignment with 'The Engineering Code of Ethics'.

5.3 Sustainability

Sustainability was concluded entirely favourably for the QUTM team, with limited environment, economic and social concerns. A triple bottom line was conducted to assess the project's potential economic, social, and environmental impacts.

Economics & Social

The project hopes to inspire greater performance within the FSAE competition allowing greater exposure, recognition, sponsorships and revenue for QUTM, being reciprocated by QUT. QUT may

recognise greater performance and subsequent priority of QUTM which may aid further performance and benefits with additional members and improved facilitates and resources. The electrical power required by the heavy computational simulations is considered negligible and an unavoidable passive QUT and personal expense. The costs associated with future on-board track testing are yet to be concluded but is highly dependent on the decided quality and accuracy of the testing apparatus. An expensive testing apparatus may be considered a sustainable investment for QUTM. Whilst strain gauges have been commonly incorporated within wind-tunnel testing to measure aerodynamic forces on models which appear relatively cheap and within the allocated project budget. Therefore, the project's benefits to namely QUTM and QUT overwhelmingly exceed its associated costs.

Environmental

The project requires significant electrical and computational power obtained through personal and QUT facilities. The project does not require new computational resources. Its main environmental impact is demonstrated through its electricity demand which is deemed unavoidable. There are slight environmental impacts produced by the transportation involved with testing apparatus and the EV4 to the track. Thus, a reliable testing apparatus will be sourced from a local vendor to reduce travel distance and frequency. Whilst testing will be conducted once to avoid shipping and reduce electric power and damages to the EV4. Overall, the project introduces several environmental and social concerns which have been mitigated regarding testing. However, the demanded electrical power is deemed negligible and unavoidable to produce the potential benefits to QUT and QUTM.

5.4 Future Work

The mentioned simulations will be reported to the QUTM team which will verify the numerical method's confidence. The numerical method requires further investigation into translational motion and related convergence issues. Possible work includes:

- Domain and Mesh refinement/improvement. There were notable problems throughout the thesis of limited mesh refinement to optimise computational time and power.
- Geometry optimisation.
- Perhaps utilising Patel's rotational method of RBM which provides greater consistency with subsequent increase in computational time.

In addition, the project and QUTM would benefit from potential yaw and on-board track testing to correlate with the results. Although the wind-tunnel testing at QUT is currently under investigation. through the small scale QUT wind tunnel which requires further investigation itself. Furthermore, the QUTM team would benefit from development of a dynamic simulation incorporating cornering characteristics such as: roll, pitch, yaw, slip-angle, steering angle, with variable cornering curvature.

Reference List

[1] QUT MOTORSPORT. EV4. Accessed https://www.qutmotorsport.com (27/10/22)

[2] Keogh, J., Doig, G., Barber, T. J., & Diasinos, S. (2014). The Aerodynamics of a cornering inverted wing in ground effect. *Applied Mechanics and Materials*, *553*, 205–210. https://doi.org/10.4028/www.scientific.net/AMM.553.205

[3] Keogh, J., Barber, T., Diasinos, S., & Doig, G. (2015). Techniques for Aerodynamic Analysis of Cornering Vehicles. *SAE Technical Papers*, *2015-March*(March). https://doi.org/10.4271/2015-01-0022

[4] Keogh, J., Barber, T., Diasinos, S., & Doig, G. (n.d.). *AIAA Member 2 Associate Professor, School of Mechanical and Manufacturing Engineering*. UNSW Australia.

[5] Okada, Y., Nouzawa, T., Okamoto, S., Fujita, T., Kamioka, T., & Tsubokura, M. (2012). Unsteady vehicle aerodynamics during a dynamic steering action: 1st report, on-road analysis. *SAE Technical Papers*. https://doi.org/10.4271/2012-01-0446

[6] Tsubokura, M., Ikawa, Y., Nakashima, T., Okada, Y., Kamioka, T., & Nouzawa, T. (2012). Unsteady Vehicle Aerodynamics during a Dynamic Steering Action: 2nd Report, Numerical Analysis. *SAE International Journal of Passenger Cars - Mechanical Systems*, *5*(1), 340–357.

[7] Keogh, J., Barber, T., Diasinos, S., & Graham, D. (2016). The aerodynamic effects on a cornering Ahmed body. Journal of Wind Engineering and Industrial Aerodynamics, 154, 34–46. https://doi.org/10.1016/j.jweia.2016.04.002

[8] Toet, W. (2013). Aerodynamics-and-aerodynamic-research-in-formula-1 (1). *The Aeronautical Journal*, *117*(1187), 1–26.

[9] Muzaferija, S. "*ADAPTIVE FINITE VOLUME METHOD FOR FLOW PREDICTION USING UNSTRUCTURED MESHES AND MULTIGRID APPROACH,"* Ph.D. dissertation, Dept. Mech. Eng. University of London. Imperial College of Science, Technology & Medicine Department of Mechanical Engineering, 1994. [Online]. Available: https://www.researchgate.net/publication/36207266_Adaptive_finite_volume_method_for_flow_prediction_using_unstructured_meshes_and_multigrid_approach

[10] Guilmineau, E., Deng, G. B., Queutey, P., & Visonneau, M. (2018). A*ssessment of hybrid LES formulations for flow simulation around the Ahmed body.* Notes on Numerical Fluid Mechanics and Multidisciplinary Design, 135, 171-176. http://doi.org/10.1007/978-3-319-60387-2_18

[11] Ansys. (2009). *ANSYS FLUENT 12.0 User's Guide - 6.2.2 Mesh Quality*. Available at: https://www.afs.enea.it/project/neptunius/docs/fluent/html/ug/node167.htm.

[12] Moukalled, F., Mangani, L., & Darwish, M. (n.d.). *Fluid Mechanics and Its Applications The Finite Volume Method in Computational Fluid Dynamics*. http://www.springer.com/series/5980

[13] Bishopa, J. E., & Sukumarb, N. (n.d.). *Polyhedral finite elements for nonlinear solid mechanics using tetrahedral subdivisions and dual-cell aggregation*.

[14] Piomelli, U., Chasnov, J.R., 1996. *Large-Eddy simulations: theory and applications, Turbulence and Transition Modelling.* Springer, Netherlands, pp. 269–336

[15] Ockerby, R. (n.d.). *DEVELOPMENT OF THE AERODYNAMIC DESIGN TOOLS & PROCESSES FOR FORMULA-SAE*.

[16] Tsubokura, M., Kitoh, K., Oshima, N., Nakashima, T., Zhang, H., Onishi, K., & Kobayashi, T. (2007). *Large Eddy Simulation of Unsteady Flow Around a Formula Car on Earth Simulator*.

[17] Patel, D., Garmory, A., & Passmore, M. (2021). The effect of cornering on the aerodynamics of a multi-element wing in ground effect. *Fluids*, *6*(1). https://doi.org/10.3390/fluids6010003

[18] Josefsson, E., Hagvall, R., Urquhart, M., & Sebben, S. (2018). Numerical Analysis of Aerodynamic Impact on Passenger Vehicles during Cornering. *SAE Technical Papers*, *2018-May*(May). https://doi.org/10.4271/2018-37-0014

[19] Keogh, J., Doig, G., Barber, T. J., & Diasinos, S. (2014). The Aerodynamics of a cornering inverted wing in ground effect. *Applied Mechanics and Materials*, *553*, 205–210. https://doi.org/10.4028/www.scientific.net/AMM.553.205

[20] Keogh, J., Doig, G., Diasinos, S., & Barber, T. (2015). The influence of cornering on the vortical wake structures of an inverted wing. *Proceedings of the Institution of Mechanical Engineers, Part D: Journal of Automobile Engineering*, *229*(13), 1817–1829. https://doi.org/10.1177/0954407015571673

[21] Piechna, J. R., Kurec, K., Broniszewski, J., Remer, M., Piechna, A., Kamieniecki, K., & Bibik, P. (2022). Influence of the Car Movable Aerodynamic Elements on Fast Road Car Cornering. *Energies*, *15*(3). https://doi.org/10.3390/en15030689

[22] SiemensSTAR-CCM+.UserGuideV13.02; Siemens: Munich, Germany, 2018.

[23] A.G. Straatman, R.J. Martinuzzi, in Engineering Turbulence Modelling and Experiments 5, 2002

[24] Lienhart, H., Stoots, C., & Becker, S. (2002). Flow and Turbulence Structures in the Wake of a Simplified Car Model (Ahmed Modell). In *New Results in Numerical and Experimental Fluid Mechanics III* (pp. 323–330). Springer Berlin Heidelberg. https://doi.org/10.1007/978-3-540-45466-3_39

[25] Ahmed, S.R., Ramm, G., Faitin, G., 1984. Some salient features of the time-averaged ground vehicle wake. SAE Technical Paper No. 840300.

[26] Hughes, T. (2018). *CFD Study of Flow over a Simplified Car (Ahmed Body) Using Different Turbulence Models*. http://www.researcgate.npublications/325451944

[27] Krajnovic, Sinisa., Chalmers tekniska högskola. Institutionen for termo och fluiddynamik., & Chalmers tekniska högskola. (2002). *Large-eddy simulations for computing the flow around vehicles*. Dept. of Thermo and Fluid Dynamics, Chalmers University of Technology.

[28] LEAP, Australia. *CFD for FSAE teams*. (Feb 26th, 2018). Accessed: April 24th, 2022. [Online Video]. Available: https://www.youtube.com/watch?v=BmLFTgmIN48&list=PLvsJbyBB0CMcLcnFTUJox3V0ib82t4drw

[29] Dharmawan, M. A., Ubaidillah, Nugraha, A. A., Wijayanta, A. T., & Naufal, B. A. (2018). Aerodynamic analysis of formula student car. *AIP Conference Proceedings*, *1931*. https://doi.org/10.1063/1.5024107

[30] Oxyzoglou, I., & Pelekasis, N. (2017). *DESIGN & DEVELOPEMENT OF AN AERODYNAMIC PACKAGE FOR A FSAE RACE CAR*.

[31] Rules, F. (2021). *Formula SAE® Rules 2022 Rules 2022*.

Appendix

Appendix A FSAE Events

The skid pad displayed in figure 18 measures the vehicle cornering ability on a flat surface while making a constant radius turn [31]. The FSAE-A rules states: the vehicle will enter perpendicular to the figure eight pad and will take one full lap on the right circle; consecutively followed by a second lap of the right cycle being timed to simulate constant cornering; the vehicle will transition to the left cycle for the third lap; followed by a fourth lap being timed [31]. Immediately upon competition the vehicle will exit the track [31]. Section D.10.3 outlines any incorrect number or sequence of laps will result in a DNF; the vehicle is allowed to stall and spin out, however, if the vehicle goes off course it qualifies as a DNF; .125 second penalties are awarded for every cone hit [31].

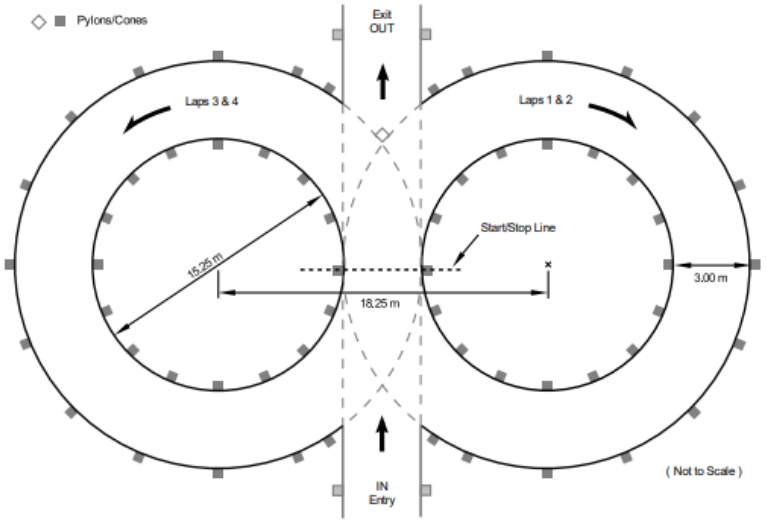

Figure 18: Skid Pad

The autocross event tests the vehicle manoeuvrability and handling qualities on a tight course [31]. Section D.11.1 discusses the course layout following specifications such as; average speeds between 40 to 48km/hr; straights no longer than 60 metres with hairpin turns at both ends with a minimum outer diameter of 9 metres; straights no longer than 40 metres with wide turns on the ends; constant turns ranging from 23 to 45 metres; slaloms in a straight line with 7.62 to 12.19 metres; miscellaneous features including chicanes, multiple turns, decreasing radius turns, etc [31].

Overall, the FSAE-A competition is significantly comprised of cornering metrics and performance. The most prominent event pertaining cornering abilities is the skid pad which aims to simulate a constant cornering environment. The autocross event features a variety of cornering conditions to evaluate overall handling abilities. Therefore, cornering performance and subsequent aerodynamics is an imperative design parameter for the EV4.

Appendix B Y+ Calculation

$$Re_x = \frac{\rho U_\infty L}{\mu}$$

$$C_f = \frac{.026}{Re_x^{\frac{1}{7}}}$$

$$\tau_{wall} = \frac{C_f \rho U_\infty^2}{2}$$

$$U_f = \sqrt{\frac{\tau_{wall}}{\rho}}$$

$$\Delta s = \frac{y^+ \mu}{U_f \rho}$$

Appendix C CFD and Cornering Equations

$$D_i = (PA_x + \tau_x|A|)\cos(\varphi) + \left(PA_y + \tau_y|A|\right)\sin(\varphi) \dots D = \sum D_i$$

$$S_i = -(PA_x + \tau_x|A|)\sin(\varphi) + \left(PA_y + \tau_y|A|\right)\cos(\varphi) \dots S = \sum S_i$$

$$P = pressure, \quad A = Cell\ Area, \quad \tau = Wall\ Shear\ Stress, \quad \varphi = cell's\ yaw\ angle$$

Velocity given at any point within the fluid-field:

$$U_\infty = \omega\sqrt{(y - y_c)^2 + (x - x_c)^2}$$

Pressure coefficient with relative U_∞:

$$C_p = \frac{p}{.5\rho U_\infty^2}$$

Yaw angle:

$$\varphi_{flow} = \tan^{-1}\left(\frac{x - x_c}{y - y_c}\right)$$

Cell Angle:

$$\varphi_{face} = \tan^{-1}(\frac{A_{fx}}{A_{fy}})$$

Cell's relative yaw angle:

$$\varphi_p = \varphi_{face} - \varphi_{flow}$$

Cell x-y area:

$$A_{fxy} = \sqrt{\left(A_{fx}\right)^2 + \left(A_{fy}\right)^2}$$

Observed cell face area:

$$A_{fo} = A_{fxy}\sin\left(\varphi_p\right)$$

Drag formulation:

$$C_D = C_{Dv} + C_{Dp}$$

Pressure Drag Change:

$$C_{Dp} = \frac{\sum C_p A_{fo}}{bc}$$

Appendix D: Ahmed Body Mesh Refinement Test

The mesh refinement table illustrated below Table … was conducted on a 5m Cornering. Refinement was dedicated towards the three body of influences in proximity and labelled respectively leading, near and wake. The large unoccupied volume of the domain was initially thought insignificant towards fluid physics on the Ahmed body. However, it was determined later through a mesh refinement test on the front wing to have significant effect on generated aerodynamic forces with a substantial increase in computational time. Whilst flow characteristics remained consistent throughout refinement. Within this test cell size was halved at the body-of-influence size increasing the number of cells from 1098455 to 67836679 with an unnoticeable increase in meshing time but substantial increase in simulation time. The finalised polyhedral mesh consisted of:

- volume at .75m
- boi-front at .05m
- boi-aft at .01m
- boi-wake at .025m
- 8 Layers of last-ratio inflation at .00058 addressing a near wall y+ of 30

Mesh	Cell Count	Mesh Time (Mins)	Cd	Cl	Cy	My	Fs	Cs	Simulation Time (Mins)
1	1098455	3	0.31	0.34	-0.06	-2.94	-5.36	-.12	31
2	6783679	7	.245	.32	-.062	-2.95	-5.23	-.11	135.5

Table 5: Mesh Refinement

Appendix E: Ahmed Body Additional Figures

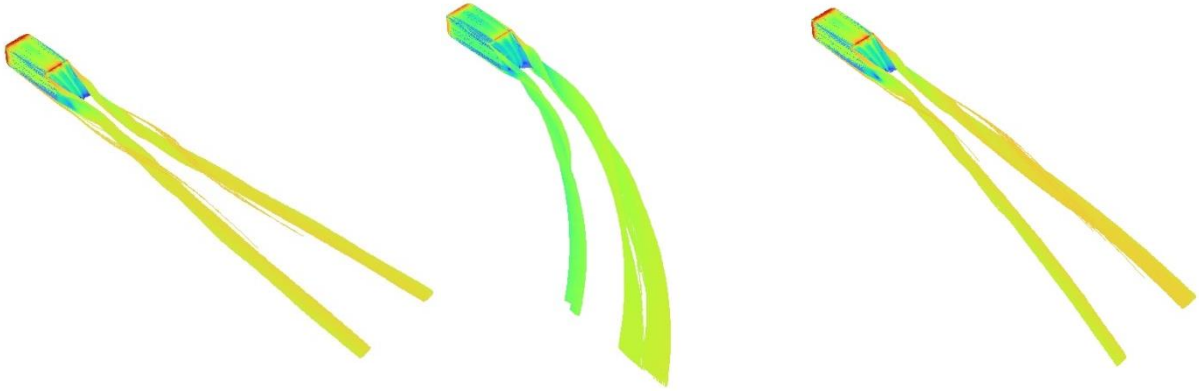

Figure 19: Pathline at 0, 5 and 20 Metres (left-right)

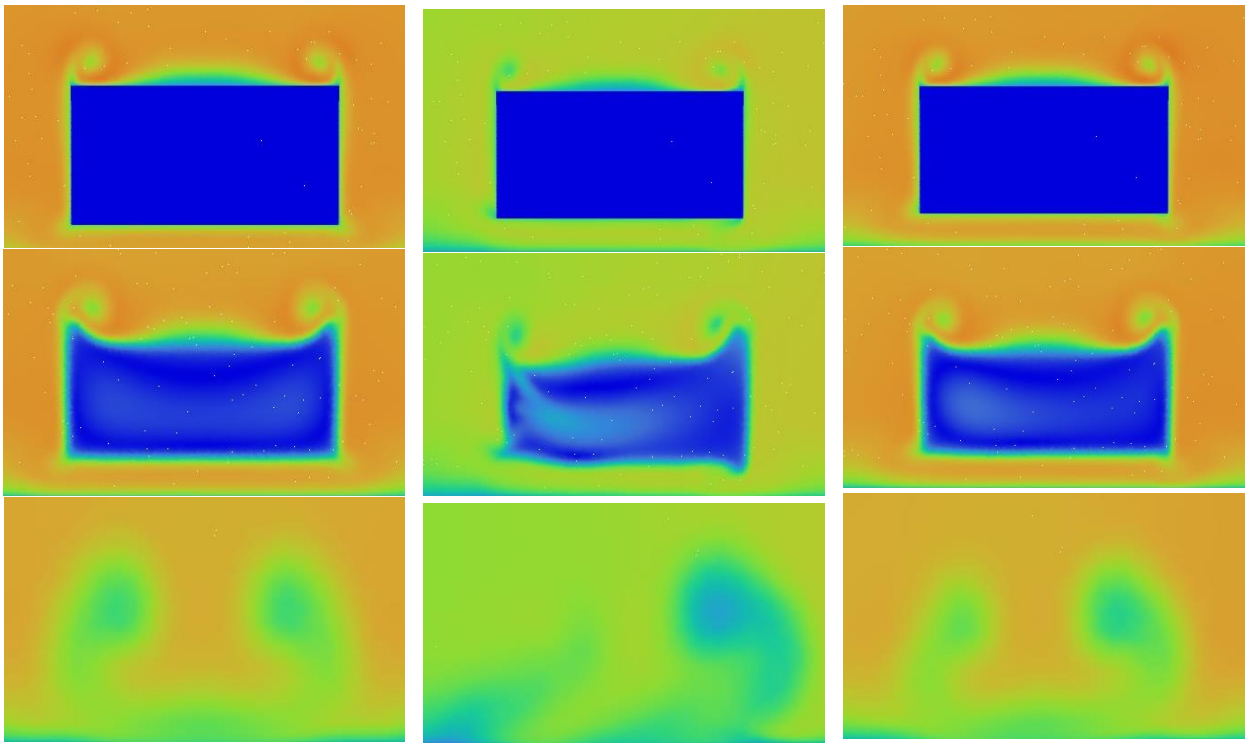

Figure 20: Wake Contours at 0, 5 and 20 metres (taken from Ahmed, x=.522, .599, 1.02)

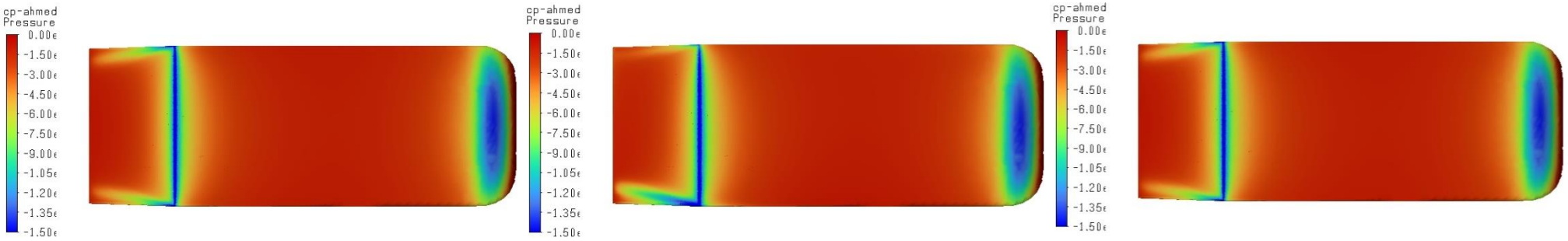

Figure 21: Pressure Coefficients at 0, 5 and 20 Metres (ranged from 0 -> -1.5)

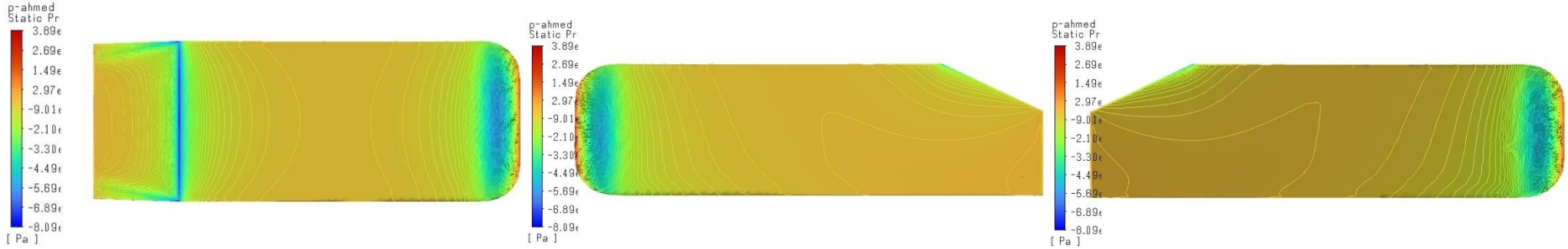

Figure 22: Ahmed Body Inboard and Outboard Pressure 0m.

Figure 23: Ahmed Body Top, Inboard and Outboard Pressure 5m.

Figure 24: Ahmed Body Inboard and Outboard Pressure 20m.

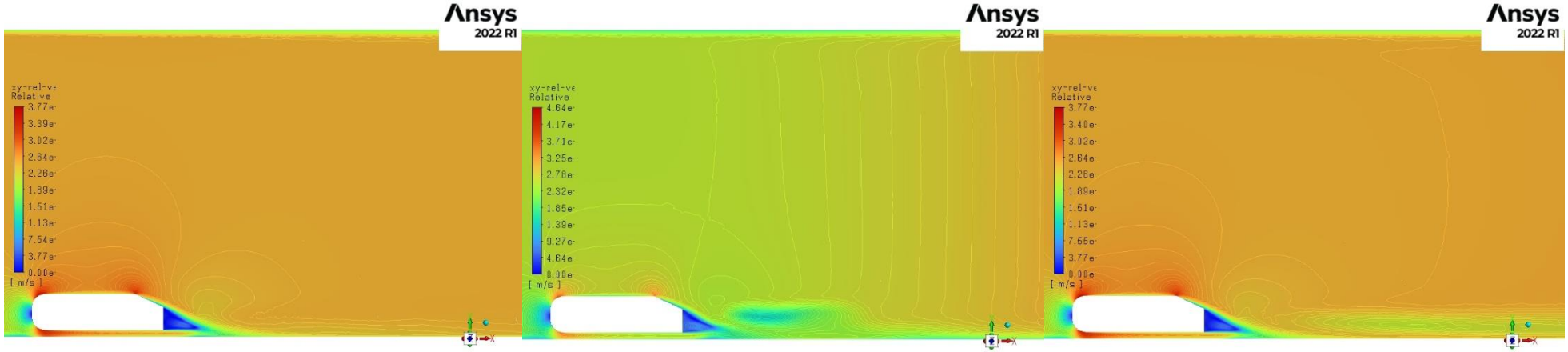

Figure 25: XY Contours at 0, 5 and 20 Metres.

Appendix F: Trailing Wake Depicted by Keough and Hughes

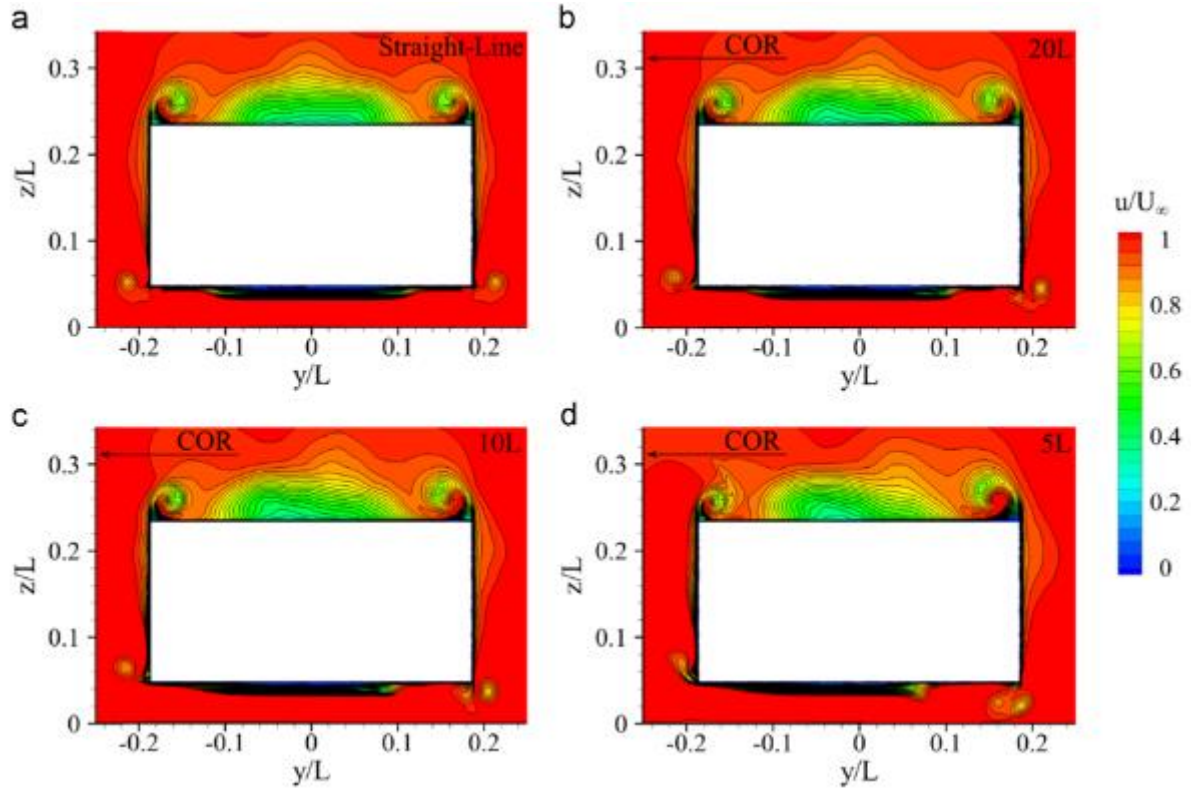

Figure 26: Keough's Wake Depiction at x=.522m.

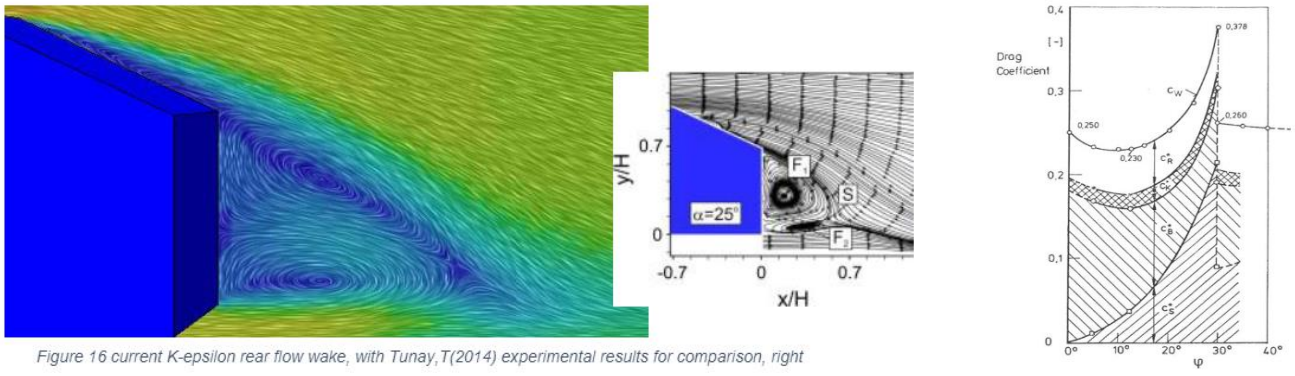

Figure 16 current K-epsilon rear flow wake, with Tunay,T(2014) experimental results for comparison, right

Figure 27: Hughes Wake and Drag on a 25-degree slant angle

Appendix G: Domain Refinement and Mesh Refinement Table

Domain (4L, 10L)	Cell Count	Cross Sectional Area	Time (minutes)		Drag	Lift	Side Force
			Mesh	Sim			
.06%	6200097	55m^2	15	95	68.589	-316.266	27.567
1.2%	5737710	18.33m^2	20	87	71.075	-328.288	-27.997
3%	5613714	11m^2	16	83	72.986	-331.969	-28.467
3% at (2.5L, 5.5L)	5527784	11m^2			72.711	-339.005	-28.168

Table 5: Domain Refinement

Mesh	Cell Count	Volume Size	Boi Size (Near.Wake)	Time (minutes)		Drag	Lift	Side Force
				Mesh	Sim			
1	5637243	.1	0.025 0.05	16	141	68.776N	-309.850N	-28.701N
2	41911179	.1	.01 .025	95	707	62.152N	-272.476N	-24.328N
3	56562190	.1	.005 .015	109	1130	64.126N	-289.987N	-23.686N
4	57987335	.05	.01 .025	111	991	61.573N	-255.165N	-25.843N

Table 6: Mesh Refinement

Appendix H: Front Wing

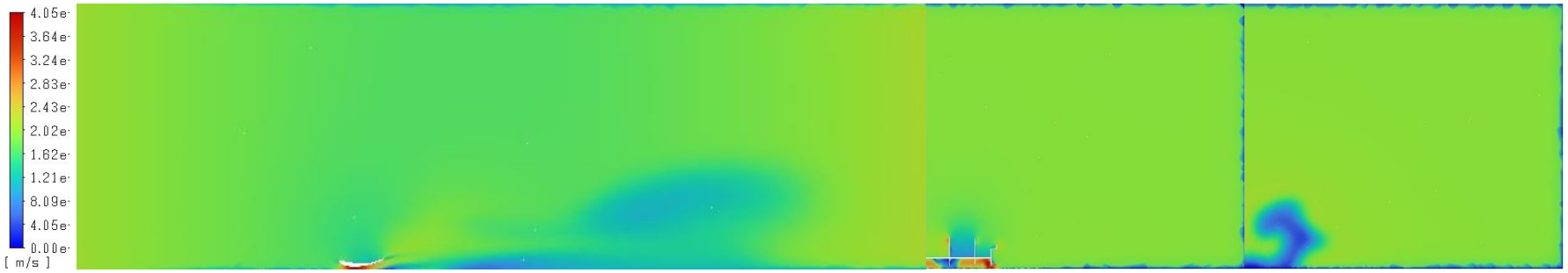

Figure 28: Translational Motion

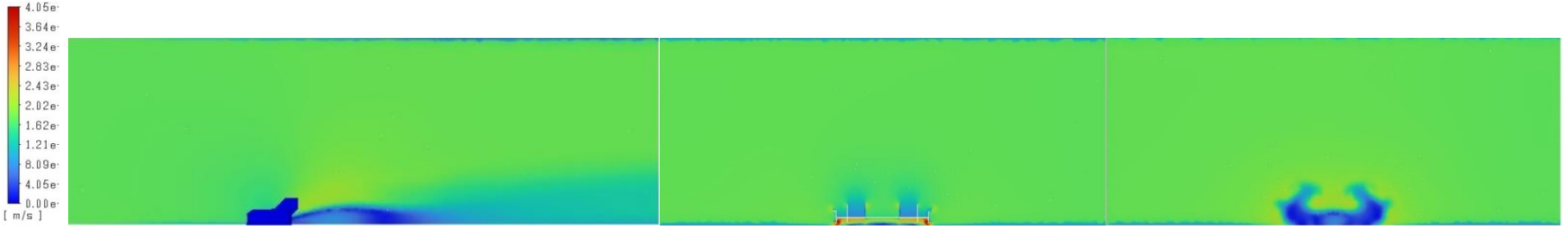

Figure 29: 0m Cornering Radius

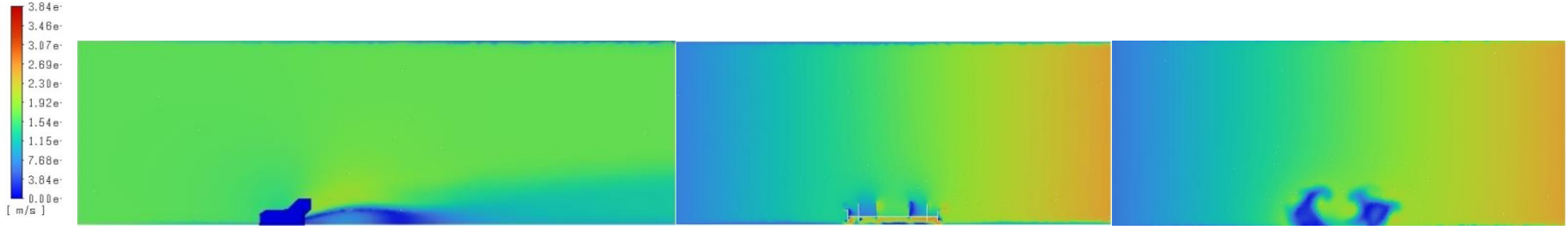

Figure 30: 5m Cornering Radius

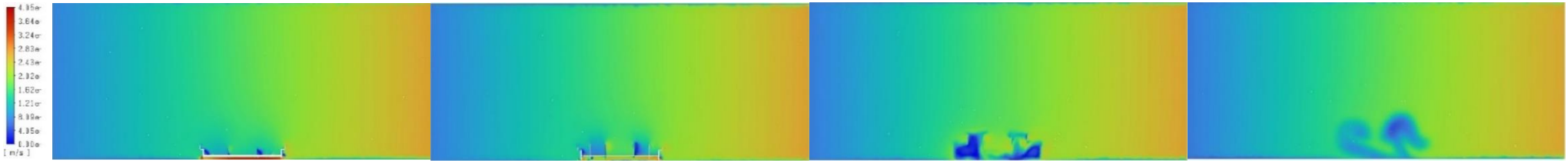

Figure 31: 5m Cornering Radius Wake Development

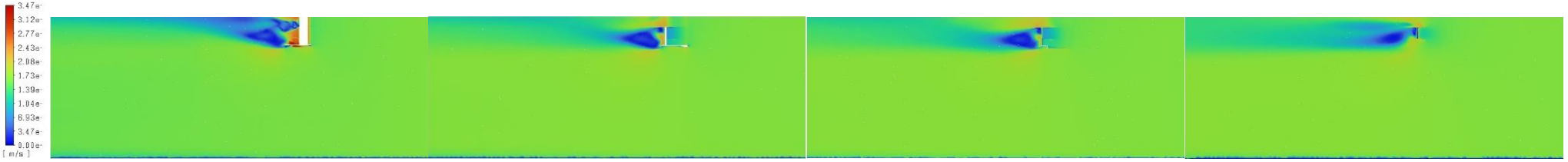

Figure 32: Translational Wake Development

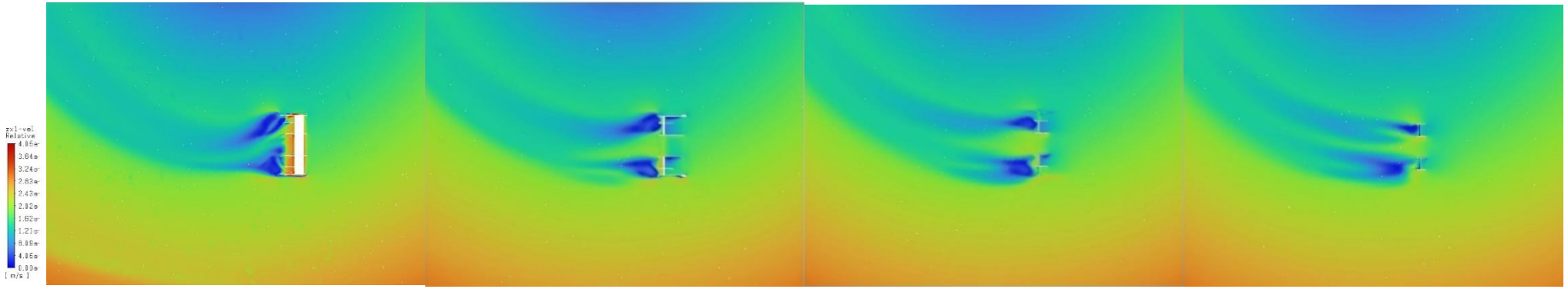

Figure 33: 5m Cornering Radius

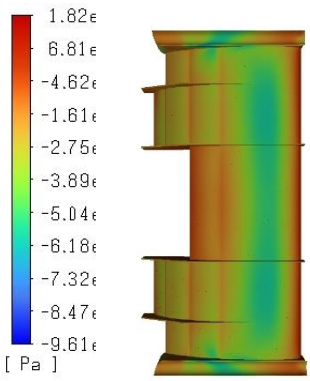

Figure 34: 0m Cornering Radius Bottom Pressure Contours

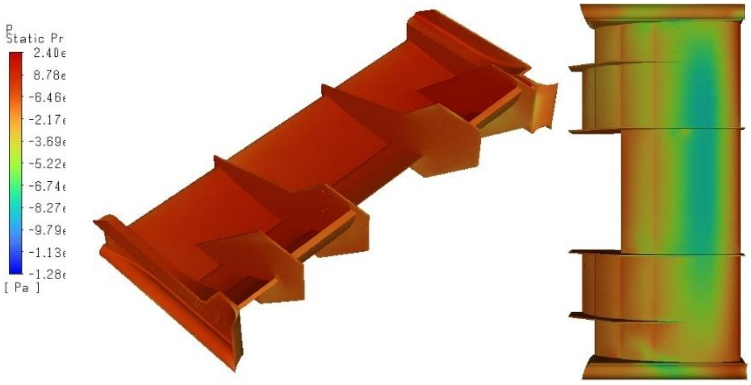

Figure 35: 5m Cornering Radius Isometric and Bottom Pressure Contours

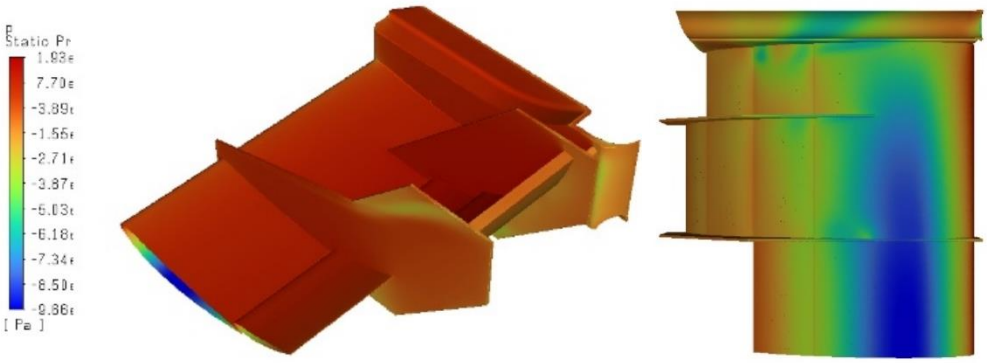

Figure 36: Verification Simulation Isometric and Bottom Pressure Contours

Appendix I: Wheels (5m Cornering Condition)

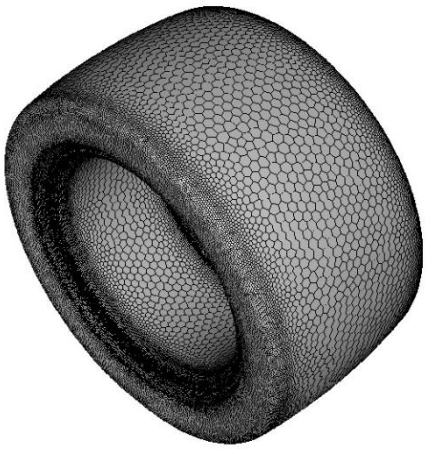

Figure 37: Replica Wheel Mesh

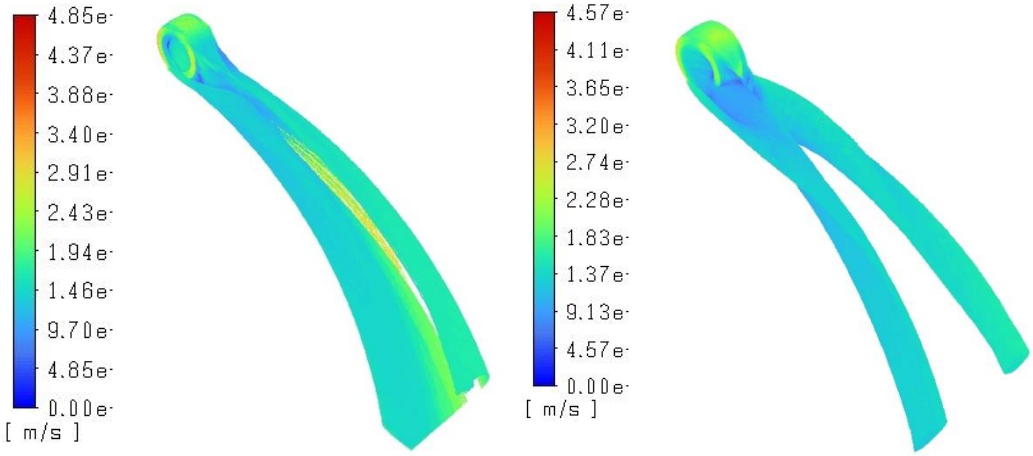

Figure 38: Simplified VS Replica Fluid-Flow

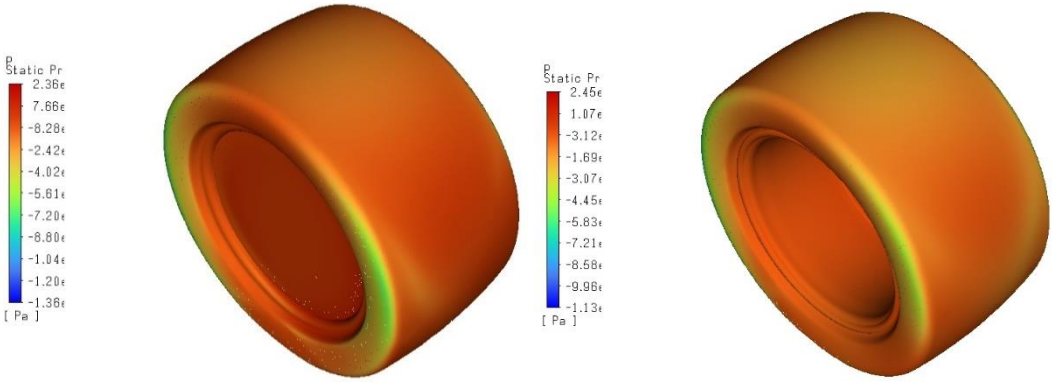

Figure 39: Simplified Vs Replica Isometric Pressure Contours

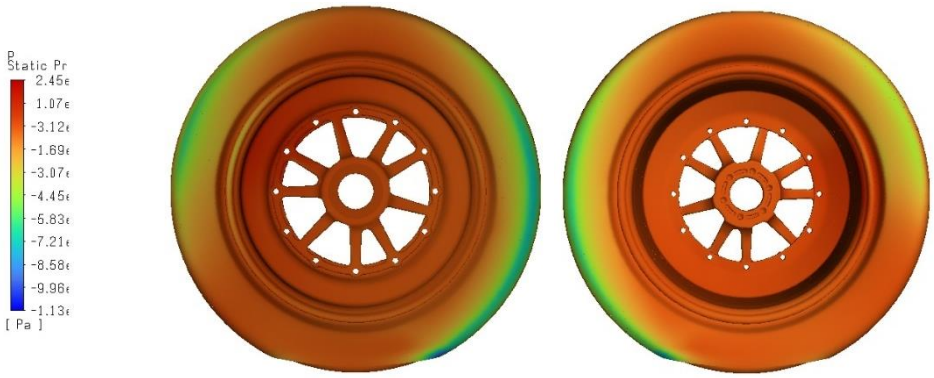

Figure 40: Replica Side Pressure Contours

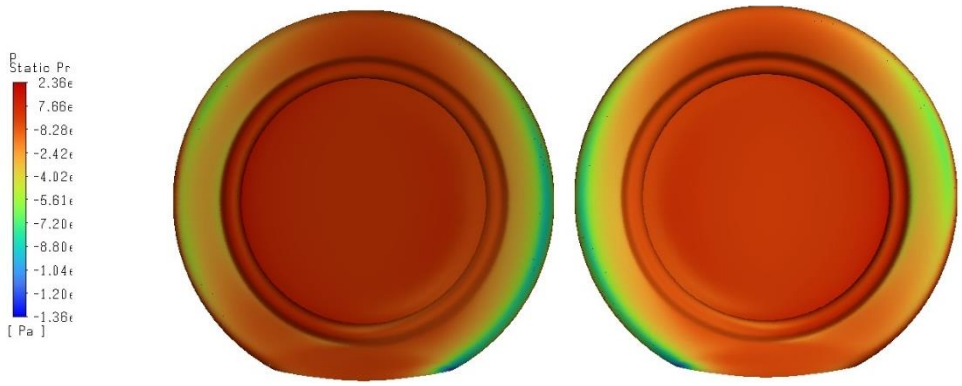

Figure 41: Simplified Side Pressure Contours

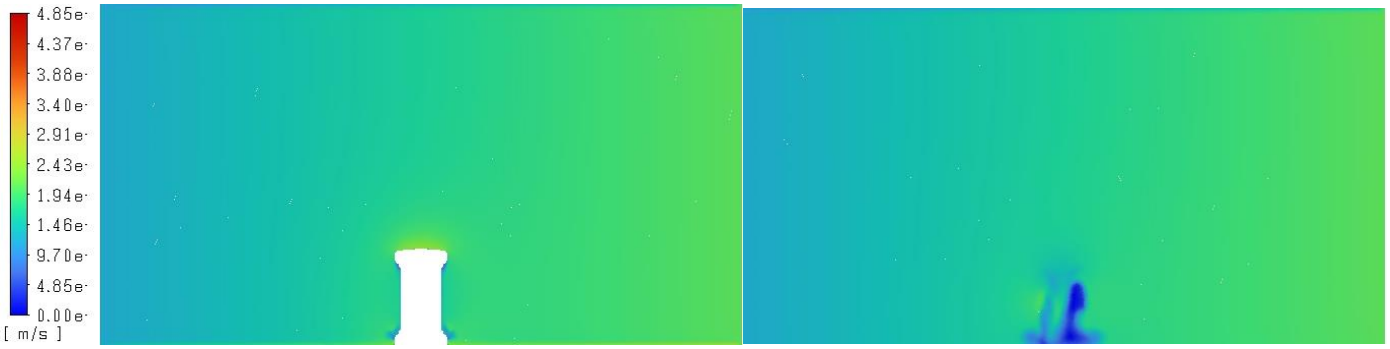

Figure 42: Simplified Trailing Wake

Figure 43: Replica Trailing Wake

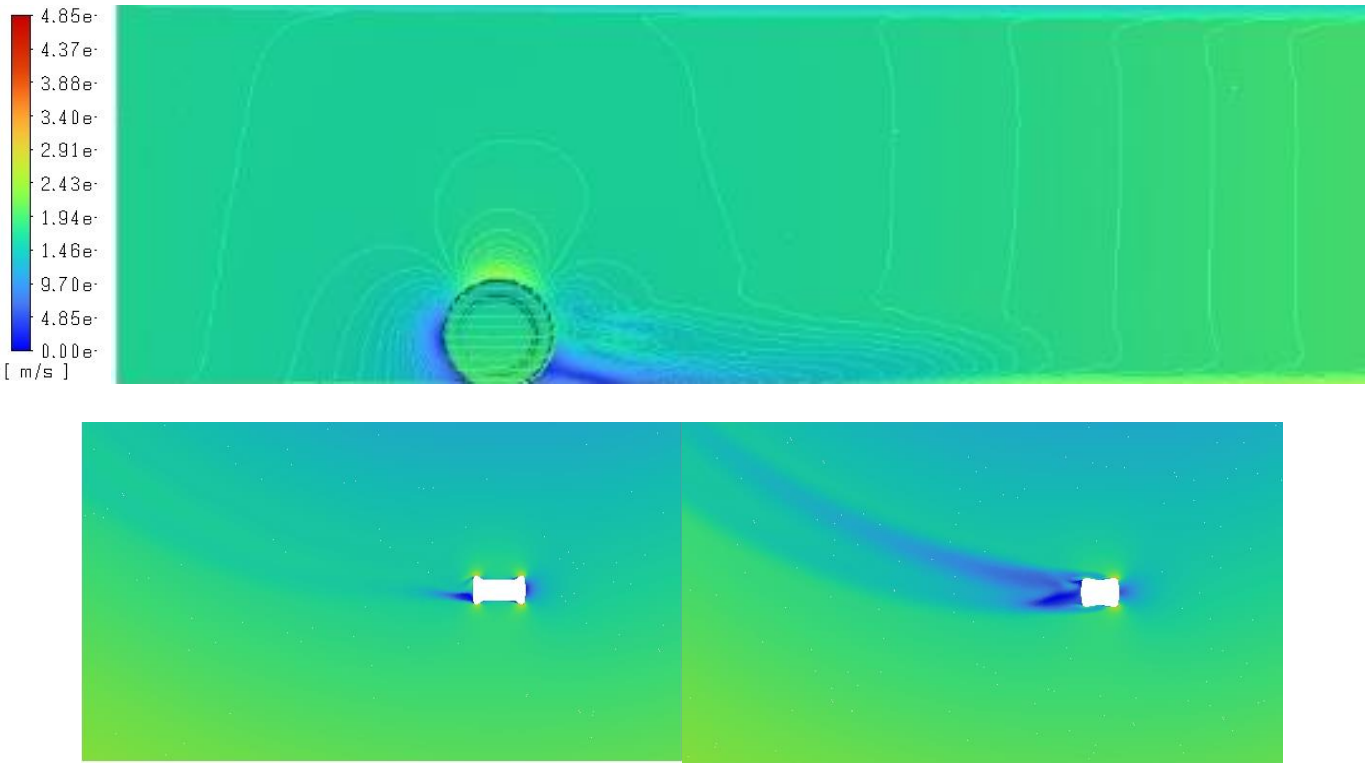

Figure 44: Simplified Velocity Contours (taken at x=0, y=.05 and y=.2)

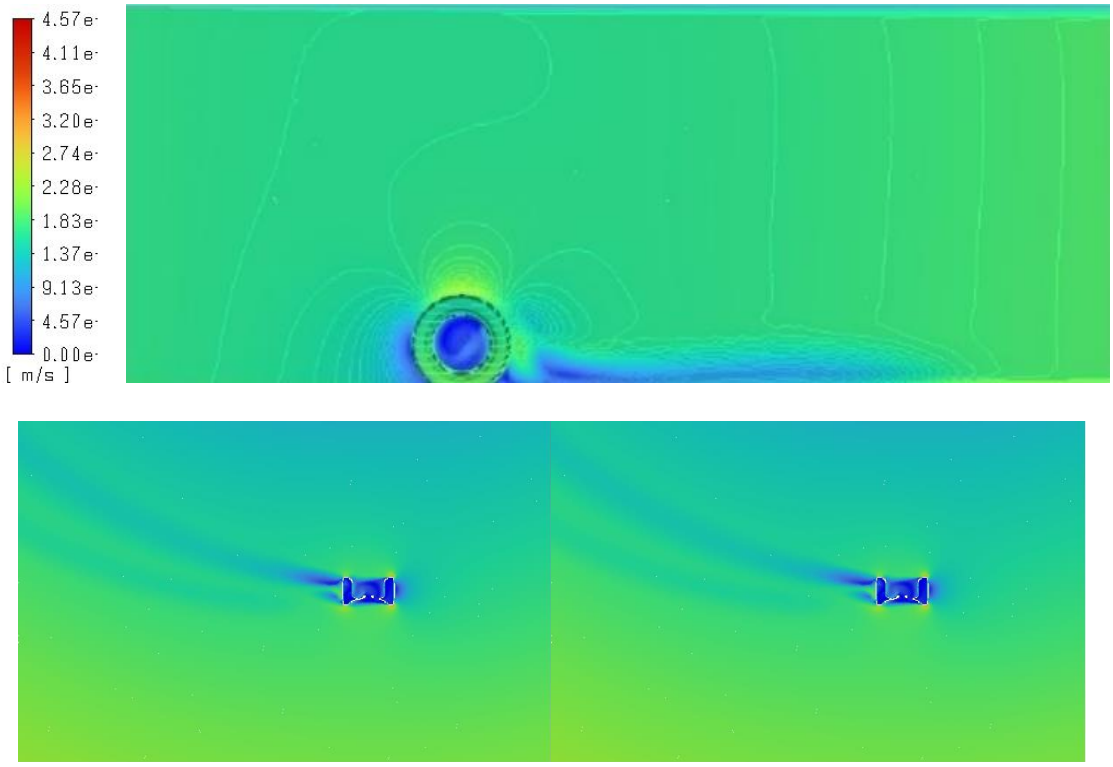

Figure 45: Replica Velocity Contours (taken at x=0, y=.05 and y=.2)

Appendix J: Chassis (5m Cornering Conditions)

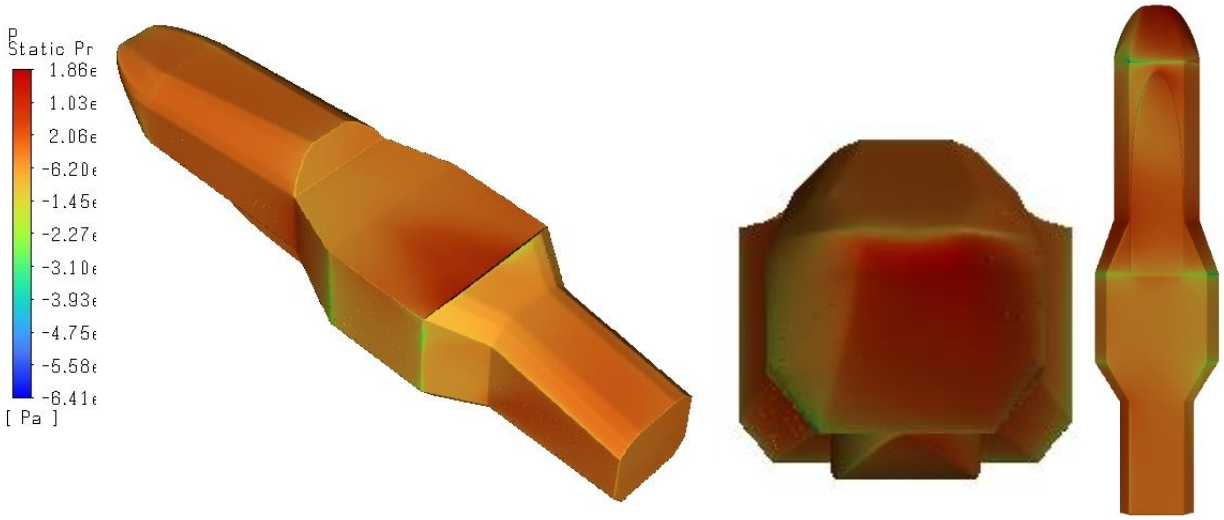

Figure 46: Chassis Pressure Contours

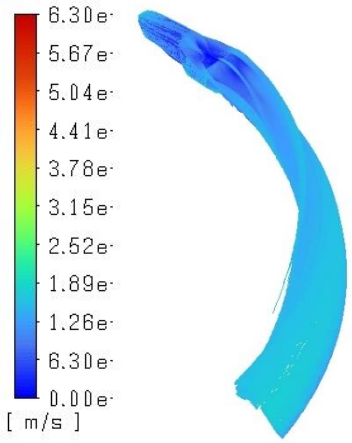

Figure 47: Chassis Fluid-Flow

Figure 48: Mid-plane Velocity Contour Chassis

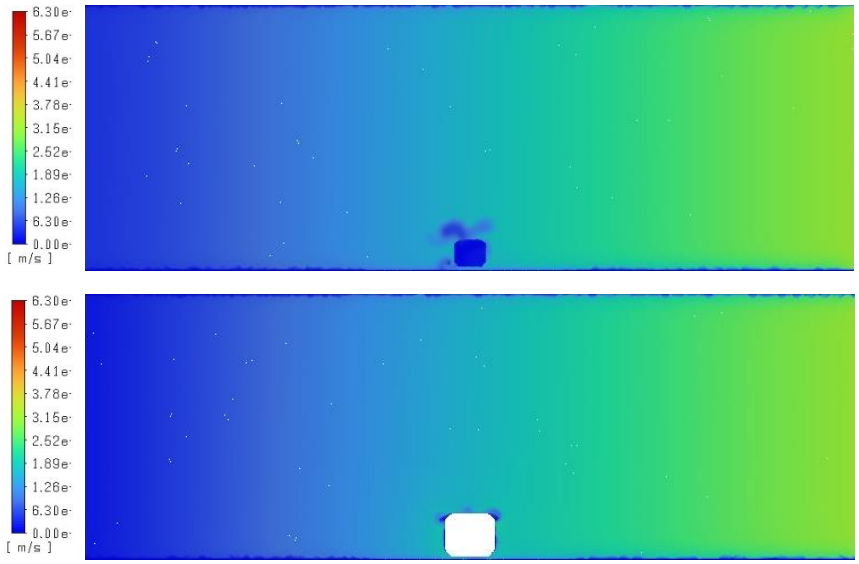

Figure 49: Chassis Trailing Wake (Mid and Aft)

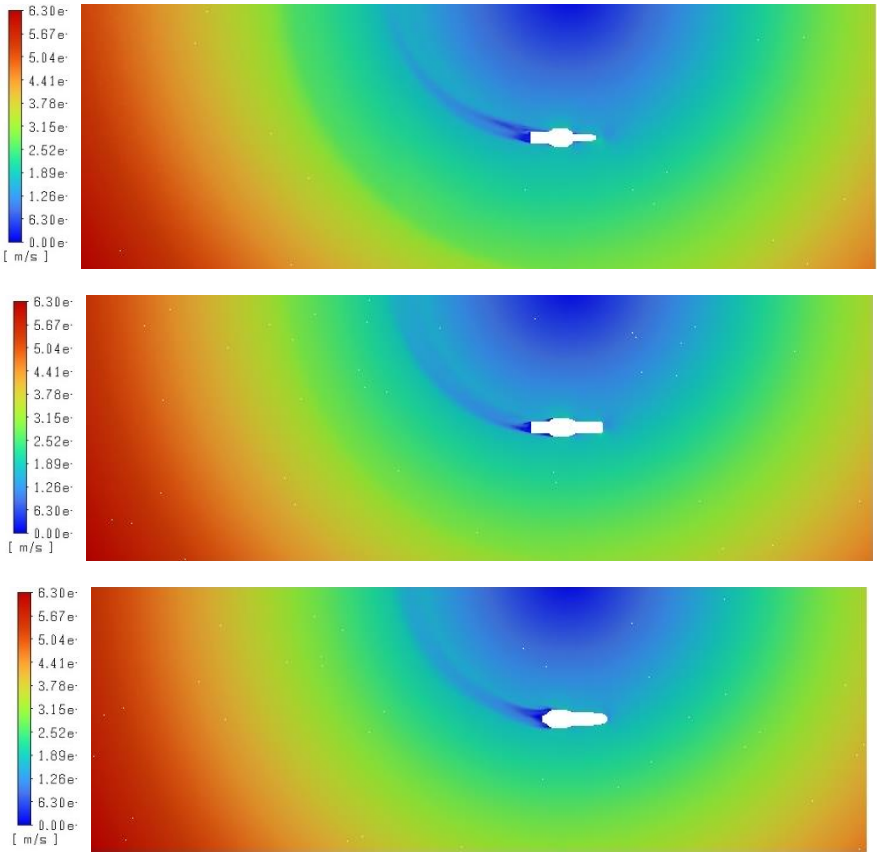

Figure 50: Wake Formation (at y=.05, .2, .45)

Appendix K: Rear Wing (5m Cornering Condition)

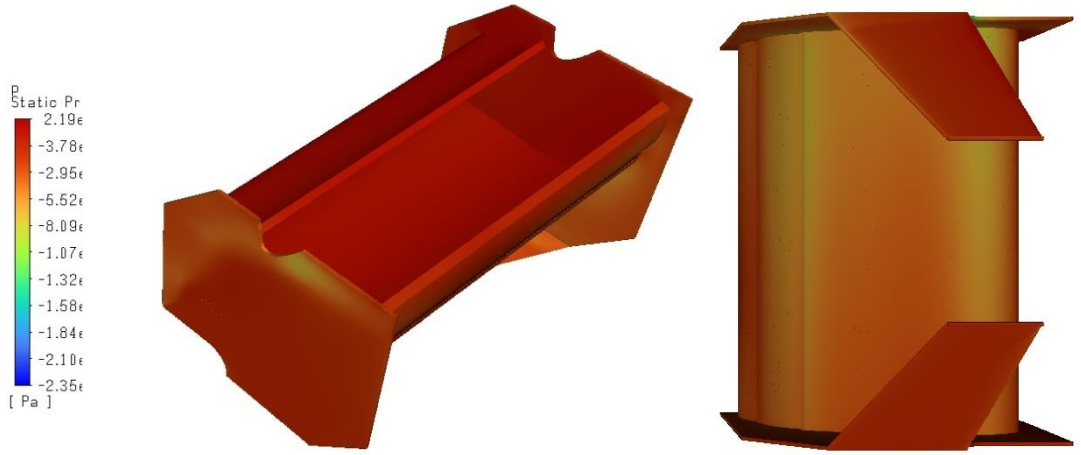

Figure 51: 5m Cornering Radius Isometric and Bottom Pressure Contours

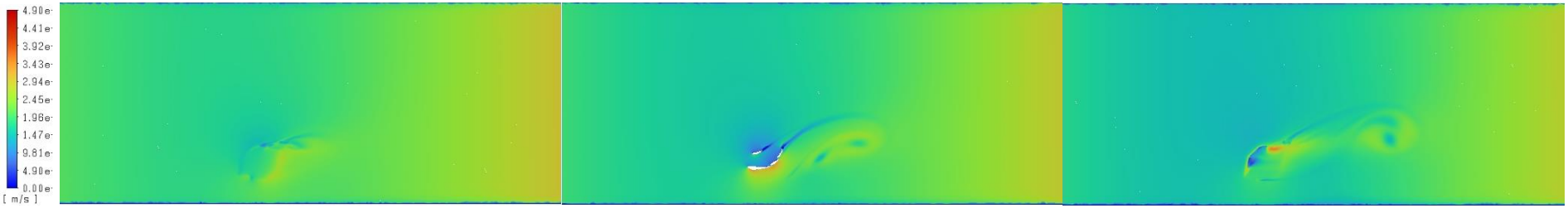

Figure 52: 5m Cornering Radius XY-Plane Velocity Contours

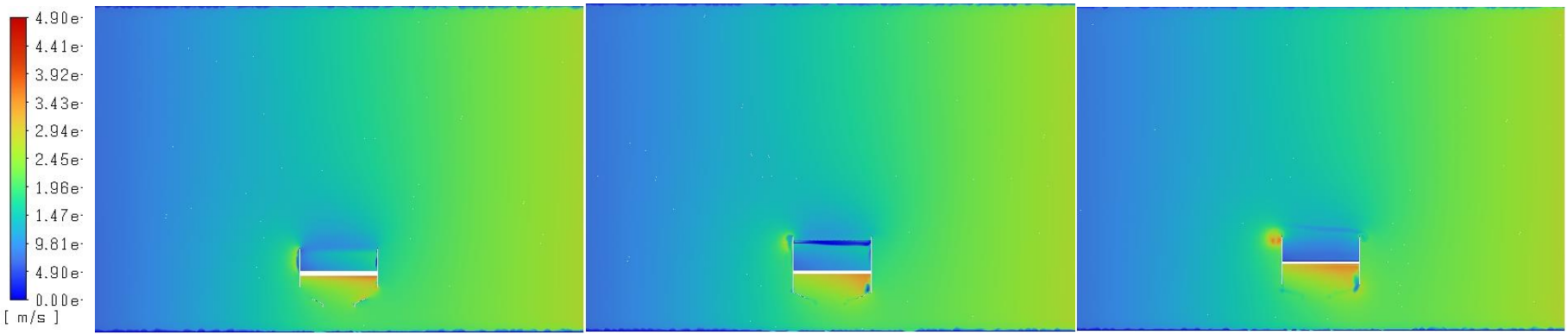

Figure 53: 5m Cornering Radius Wake Development

Appendix L: Associated Cornering Conditions Calculations

The wheel's outer radius was measured in Space Claim approximately at .203metres with a total circumference of 1.276metres.

Angular velocity was determined based on the rolling road and fluid flow velocity illustrated in the equation below:

$$\omega = \frac{v}{c} \times 2\pi$$

The most applicable cornering situations for the QUTM team are exhibited through the Skid Pad and Autocross Event. Appendix A contains additional information and specifications of the associated cornering radii and velocity. The Skid Pad Event utilises an inner cornering radius of 8 metres. With an appropriate cornering radius of 9 metres at a maximum tangential velocity of 11m/s calculated through the equation below with a frictional coefficient of 1.4:

$$\mu_S g = \frac{v^2}{r}$$

Whilst corners described in the Autocross Event of 23 and 45 metres were calculated with a maximum tangential velocity of respectively 17.5 and 24.5 m/s. The wheels require an angular velocity of 86 and 121rad/s with domain rotation set at 1.23 and .76 rad/s.

Appendix M: EV at 16.67m/s with a cornering radius of 5 with Rolling Wheels

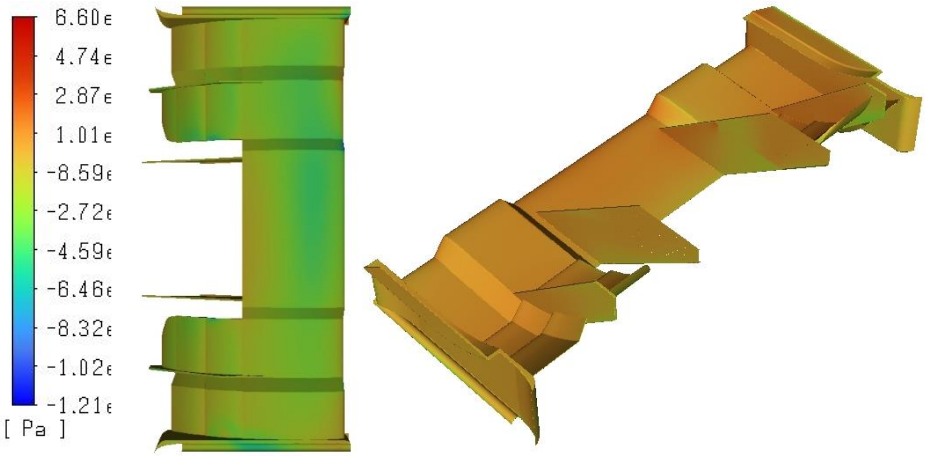

Figure 54: Pressure Contours EV Simulations with Rolling Wheels

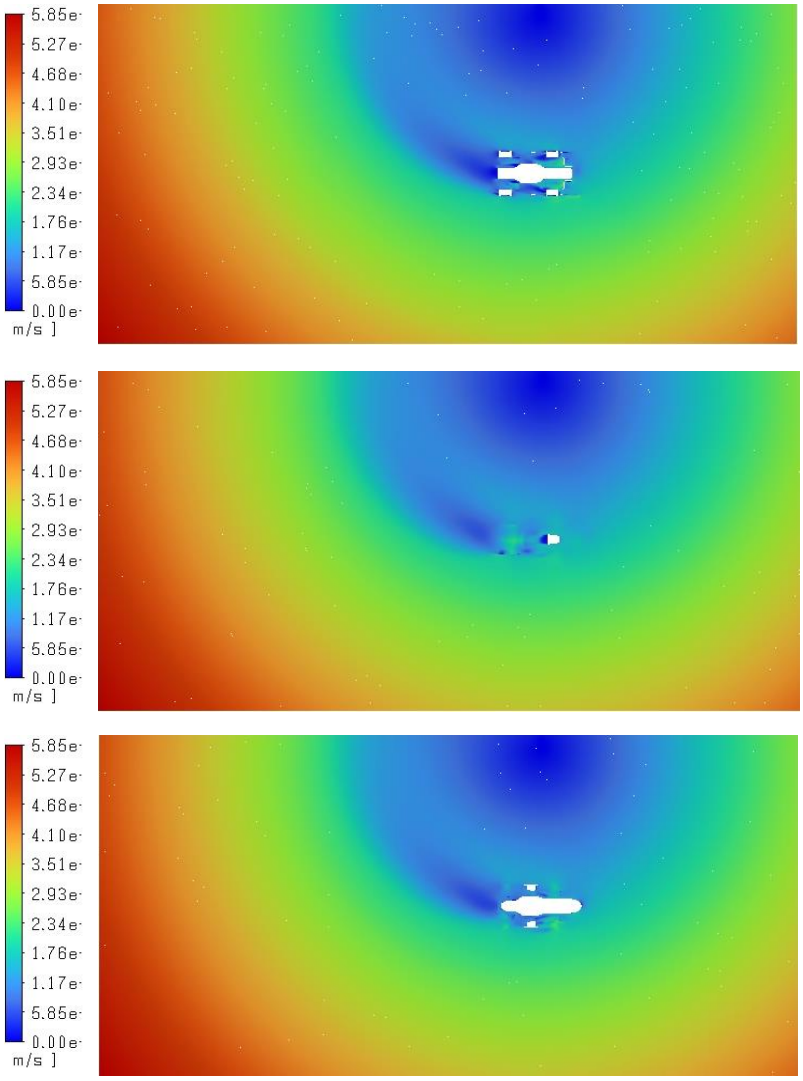

Figure 55: Velocity Contours EV Simulations with Rolling Wheels (taken at x=.25, .5, .7)

Appendix N: EV 16.67m/s with a cornering radius of 5, 20 and 40 metres

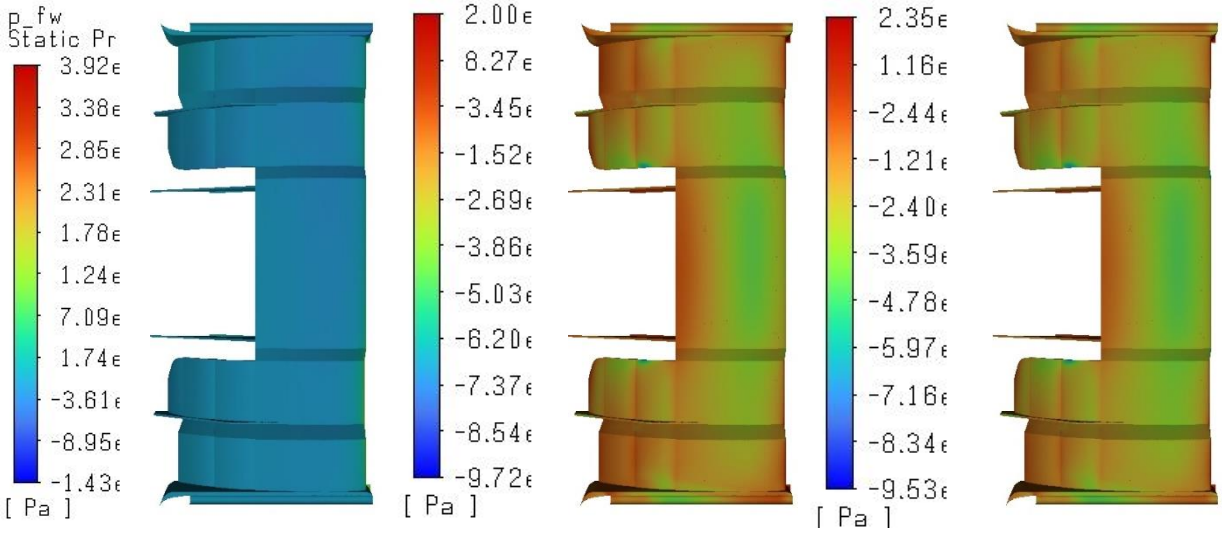

Figure 56: Pressure Contours between 0, 5 and 20 metre Cornering Radii

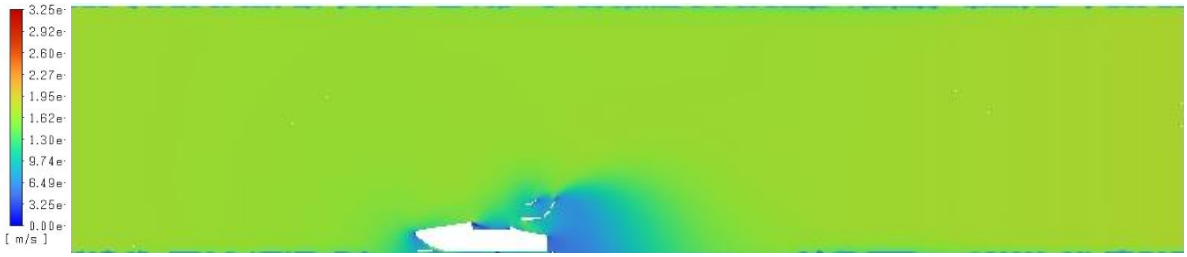

Figure 57: XY-Plane Velocity Contour 5 metre Cornering Radius

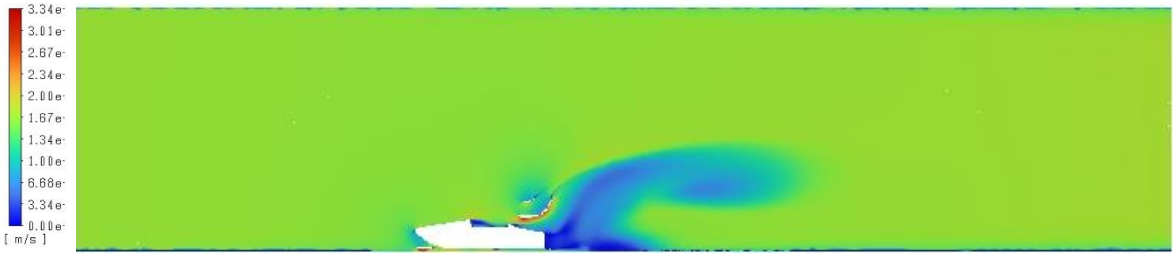

Figure 58: XY-Plane Velocity Contour 20 metre Cornering Radius

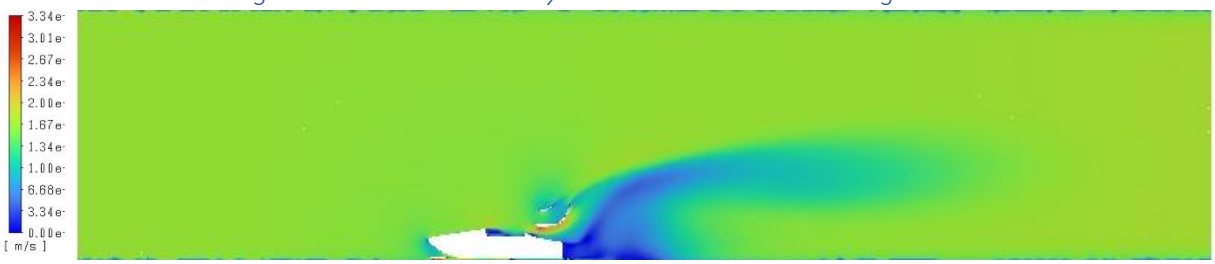

Figure 59: XY-Plane Velocity Contour 40 metre Cornering Radius

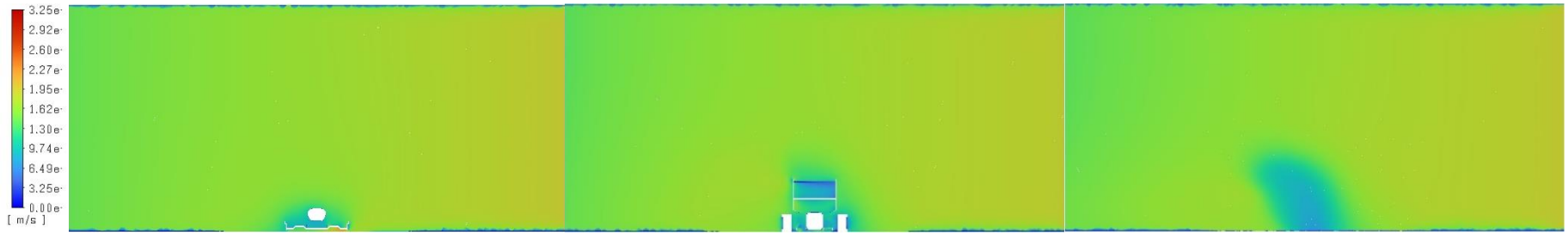

Figure 60: Wake Formation 5m Cornering Radius

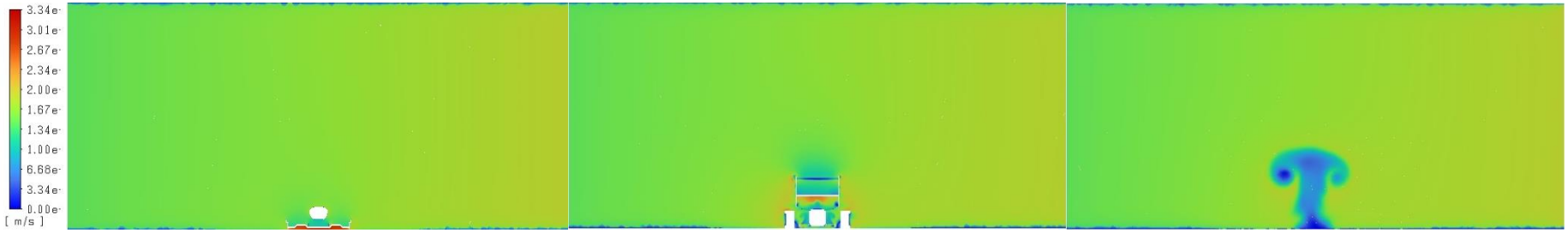

Figure 61: Wake Formation 20m Cornering Radius

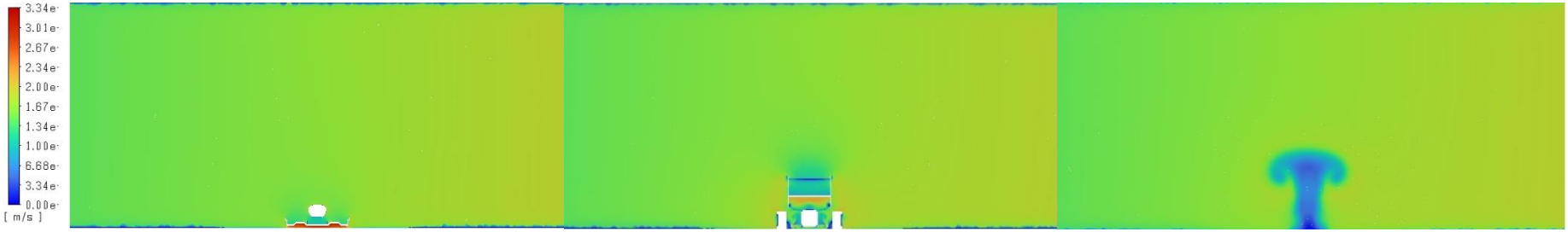

Figure 62: Wake Formation 40m Cornering Radius

Forces

	Forces [N]		
Zone	Pressure	Viscous	Total
c	(45.577799 8.6523851 12.354229)	(3.7412704 0.17454324 -0.020645234)	(49.319069 8.8269283 12.333583)
floor	(0 -519.28921 0)	(225.12794 0 141.31618)	(225.12794 -519.28921 141.31618)
flw	(19.990827 1.8316136 -3.8221246)	(0.62971248 0.13570993 -0.029518974)	(20.62054 1.9673235 -3.8516435)
frw	(11.945916 5.2252357 2.6441322)	(0.421451 0.087426219 -0.00024857862)	(12.367367 5.3126619 2.6438836)
fw	(72.073079 -136.72767 -34.525973)	(7.09582 0.85886038 -0.41510668)	(79.168899 -135.86881 -34.941079)
lsw	(1.9690571 -10.925864 0.64439806)	(0.37313516 -0.024839193 0.0066075601)	(2.3421923 -10.950703 0.65100562)
nc	(35.971712 23.242984 -17.184515)	(1.77845 0.025317613 -0.28549426)	(37.750162 23.268301 -17.47001)
rlw	(5.003617 5.8256956 -3.012355)	(0.19103054 -2.927775e-05 -0.033235884)	(5.1946475 5.8256663 -3.0455909)
roof	(8.0672649e-15 927.67462 0)	(164.91561 -2.9711457e-16 124.69617)	(164.91561 927.67462 124.69617)
rrw	(32.077469 2.9552912 21.586709)	(0.64466738 -0.037146426 0.16610682)	(32.722136 2.9181448 21.752816)
rsw	(6.2451593 -12.51507 5.8521624)	(1.0621538 0.041300537 0.020399804)	(7.3073131 -12.47377 5.8725622)
rw	(132.1965 -166.30934 105.16305)	(7.0843907 1.1333788 0.46179762)	(139.2809 -165.17596 105.62485)
ut	(7.0116624 -96.293904 5.8653227)	(1.8275207 0.061138307 -0.026963182)	(8.839183 -96.232765 5.8383595)
wheel-radii	(0.82497993 1.6188703 0.24076419)	(0.018573948 -0.00076598129 0.00054771084)	(0.84355388 1.6181043 0.2413119)

Figure 63: Aerodynamic Forces 5m Cornering Radius

Moments - Moment Center (0 0.5 0)

	Moments [N m]		
Zone	Pressure	Viscous	Total
c	(-2.5273555 -4.6769024 30.215181)	(-0.04023796 -0.16828599 -0.079449452)	(-2.5675934 -4.8451884 30.135732)
floor	(-827.91949 0 916.02143)	(-70.658088 -2364.5177 112.56397)	(-898.57758 -2364.5177 1028.5854)
flw	(0.033302589 11.38933 5.1618164)	(-0.07690814 0.3986656 0.029585957)	(-0.043605551 11.787996 5.1914024)
frw	(2.4030182 -6.4117522 0.8856196)	(0.05262382 -0.26286401 0.039133219)	(2.455642 -6.6746162 0.92475282)
fw	(3.6926863 -30.628265 176.94931)	(-0.014055912 0.8378208 1.7897754)	(3.6786304 -29.790444 178.73909)
lsw	(5.758617 0.87801734 -2.1330628)	(0.015206587 0.20897596 0.041482755)	(5.7738236 1.0869933 -2.0915801)
nc	(1.7635615 -20.321002 -24.764122)	(0.012014737 -0.29286398 0.13988985)	(1.7755762 -20.613866 -24.624232)
rlw	(-2.6734126 6.0037523 7.2319741)	(0.0092926105 0.14594266 0.040562013)	(-2.66412 6.1496949 7.2725361)
roof	(765.12589 -3.1814428e-16 -246.21711)	(561.13275 -2264.6037 -742.12026)	(1326.2586 -2264.6037 -988.33737)
rrw	(-4.4580997 -41.659842 12.737932)	(-0.062844299 -0.55956605 0.090504382)	(-4.520944 -42.219408 12.828436)
rsw	(-7.5325689 -5.0199385 -2.7601976)	(0.025450105 -0.62400518 0.12893389)	(-7.5071188 -5.6439437 -2.6312637)
rw	(31.192517 -107.60719 -228.41242)	(0.1764529 -1.4917203 -0.7161434)	(31.36897 -109.09891 -229.12857)
ut	(-7.4928393 -4.5372857 -24.730848)	(0.026240135 -0.2046924 0.83199697)	(-7.4665992 -4.7419781 -23.898851)
wheel-radii	(-0.22527213 -0.44946536 0.90073525)	(-0.0006441771 -0.0078473803 0.0095313215)	(-0.22591631 -0.45731274 0.91026657)

Figure 64: Moments 5m Cornering Radius

Forces

	Forces [N]		
Zone	Pressure	Viscous	Total
c	(30.569354 14.400442 6.936589)	(2.0173437 0.0062498954 -0.021658939)	(32.586698 14.406692 6.91493)
floor	(0 9.5270367 0)	(108.55471 0 15.642085)	(108.55471 9.5270367 15.642085)
flw	(4.9662459 7.0581273 -0.16700414)	(0.16752669 0.05926572 -0.0051228828)	(5.1337726 7.117393 -0.17212702)
frw	(4.2671856 7.7753447 -0.42744301)	(0.16733747 0.099086917 -0.0089465159)	(4.4345231 7.8744316 -0.43638952)
fw	(38.888378 -208.04976 -4.5115425)	(2.6798854 0.45371139 -0.044895883)	(41.568263 -207.59605 -4.5564384)
lsw	(2.1066962 -6.0582501 -0.89925524)	(0.3621563 0.017343532 0.0032874993)	(2.4688525 -6.0409066 -0.89596774)
nc	(8.4726873 8.5148597 -1.2098927)	(0.29305384 0.018171847 -0.024037896)	(8.7657411 8.5330316 -1.2339306)
rlw	(9.4523124 10.532901 -5.1284985)	(0.27426389 0.043380619 -0.065638696)	(9.7265763 10.576282 -5.1941372)
roof	(5.1266386e-15 536.29008 0)	(105.56554 -2.0389531e-16 16.589128)	(105.56554 536.29008 16.589128)
rrw	(9.6946272 9.731472 9.6269553)	(0.26897711 0.054241265 0.080439116)	(9.9636043 9.7857133 9.7073944)
rsw	(1.9808385 -4.2725451 2.2350314)	(0.35232152 0.025441683 0.013292144)	(2.3331601 -4.2471034 2.2483235)
rw	(126.42978 -250.33592 18.550016)	(3.408785 1.1742697 0.071397875)	(129.83857 -249.16165 18.621414)
ut	(7.6491159 -115.95196 1.3145298)	(2.7401964 0.080329973 0.019651565)	(10.389312 -115.87163 1.3341814)
wheel-radii	(1.4182263 1.8071519 0.1069162)	(0.019932026 0.0002050866 0.0011272169)	(1.4381584 1.807357 0.10804342)

Figure 65: Aerodynamic Forces 20m Cornering Radius

Moments - Moment Center (0 0.5 0)

	Moments [N m]		
Zone	Pressure	Viscous	Total
c	(-1.3957931 -1.7351125 41.495101)	(-0.011353041 -0.0080333559 0.40474604)	(-1.4071462 -1.7431458 41.899847)
floor	(-115.19165 0 676.94465)	(-7.8210427 -341.08286 54.277356)	(-123.01269 -341.08286 731.222)
flw	(-4.3716122 3.2288735 -2.2324495)	(-0.030289964 0.10193121 0.0012445983)	(-4.4019022 3.3308047 -2.2312049)
frw	(5.0222816 -3.2011595 -2.828859)	(0.059712993 -0.11095695 -0.022521224)	(5.0819945 -3.3121164 -2.8513802)
fw	(-0.95406169 -5.9204264 253.16886)	(0.039368717 -0.1118065 0.61294212)	(-0.91469298 -6.0322329 253.7818)
lsw	(3.8251153 1.2564215 -1.4970972)	(-0.0098207271 0.21008621 0.051444858)	(3.8152946 1.4665077 -1.4456523)
nc	(0.10539008 -1.4128212 -9.59996)	(0.0030106688 -0.030911849 0.012160373)	(0.10840075 -1.4437331 -9.5877996)
rlw	(-5.07358 10.769116 13.200051)	(-0.010931567 0.22458745 0.095894928)	(-5.0845115 10.993703 13.295946)
roof	(151.38837 -7.9641563e-16 -622.19929)	(74.651075 -348.96181 -475.04492)	(226.03945 -348.96181 -1097.2442)
rrw	(3.1440844 -15.213126 12.490919)	(0.013731541 -0.23207126 0.1044121)	(3.1578159 -15.445198 12.595332)
rsw	(-3.114557 -1.3325196 -1.1226033)	(0.013252413 -0.20953315 0.051537485)	(-3.1013046 -1.5420527 -1.0710658)
rw	(8.262872 -15.672218 -312.61798)	(-0.019358547 -0.072028373 0.52453428)	(8.2435135 -15.744246 -312.09345)
ut	(-0.82735599 -1.2377155 -21.767417)	(-0.011790929 -0.041627912 1.252187)	(-0.83914692 -1.2793434 -20.51523)
wheel-radii	(-0.13994364 -0.12171862 1.2993961)	(-0.00030216272 -0.0014864765 0.0092970476)	(-0.1402458 -0.12320509 1.3086932)

Figure 66: Moments Forces 20m Cornering Radius

	Forces [N]		
Zone	Pressure	Viscous	Total
c	(28.94949 11.499505 2.0271089)	(2.0059977 -0.0093749636 -0.0053245758)	(30.955488 11.49013 2.0217843)
floor	(0 53.670226 0)	(107.09509 0 7.5773167)	(107.09509 53.670226 7.5773167)
flw	(4.9298694 7.1208255 0.15436812)	(0.16741779 0.070202068 0.0016731216)	(5.0972872 7.1910276 0.15604124)
frw	(4.4281876 7.5440465 -0.37195531)	(0.16508933 0.091189818 -0.0068389023)	(4.593277 7.6352363 -0.37879421)
fw	(38.706962 -208.01099 -2.6960557)	(2.6633869 0.44428622 -0.024349186)	(41.370348 -207.5667 -2.7204049)
lsw	(2.034854 -6.4789431 -0.60499375)	(0.36488839 0.014250768 -0.0052595939)	(2.3997424 -6.4646923 -0.61025334)
nc	(8.5552146 8.4404092 -0.72854014)	(0.29103017 0.018208076 -0.013469459)	(8.8462447 8.4586172 -0.7420096)
rlw	(9.9273978 10.030658 -4.7083875)	(0.28562981 0.039569076 -0.066137675)	(10.213028 10.070227 -4.7745252)
roof	(5.1723677e-15 490.46407 0)	(101.42717 -1.9873124e-16 7.6774986)	(101.42717 490.46407 7.6774986)
rrw	(9.7004157 9.9843152 7.605705)	(0.2746251 0.050158053 0.077228684)	(9.9750408 10.034473 7.6829337)
rsw	(1.9756869 -4.9913288 1.5915619)	(0.35232875 0.022109361 0.010359421)	(2.3280157 -4.9692194 1.6019213)
rw	(131.92795 -247.38943 9.2104846)	(4.1538971 1.198312 0.049614762)	(136.08185 -246.19112 9.2600994)
ut	(7.2770357 -114.42641 0.71192668)	(2.6692941 0.075263313 0.0051926419)	(9.9463298 -114.35114 0.71711932)
wheel-radii	(1.3921455 1.7779604 0.069121035)	(0.020063289 0.00028958508 0.00057073378)	(1.4122087 1.7782499 0.069691768)

Figure 67: Aerodynamic Forces 40m Cornering Radius

Moments - Moment Center (0 0.5 0)

	Moments [N m]		
Zone	Pressure	Viscous	Total
c	(-0.45327471 -0.80623456 41.189168)	(-0.0046286825 -0.013370387 0.40889484)	(-0.45790339 -0.81960495 41.598063)
floor	(-56.0926 0 861.83987)	(-3.7886583 -163.74754 53.547546)	(-59.881258 -163.74754 915.38742)
flw	(-4.5123982 3.3997438 -2.2769973)	(-0.039170777 0.10566116 -0.0058474753)	(-4.5515689 3.505405 -2.2828448)
frw	(4.8525086 -3.2575377 -2.6563134)	(0.054053812 -0.10800365 -0.01830463)	(4.9065624 -3.3655413 -2.674618)
fw	(-0.053364277 -3.4457617 253.09211)	(0.02276128 -0.061044688 0.61550636)	(-0.030602998 -3.5068064 253.70761)
lsw	(3.9649288 1.1737712 -1.55825)	(-0.0069082997 0.21401756 0.05028429)	(3.9580205 1.3877888 -1.5079657)
nc	(0.066707084 -0.8478657 -9.4976054)	(0.0017017157 -0.01731632 0.011933648)	(0.0684088 -0.86518202 -9.4856718)
rlw	(-4.9150868 10.707625 12.854871)	(-0.0080115406 0.23393643 0.094394331)	(-4.9230984 10.941561 12.949265)
roof	(108.56334 -6.9865878e-16 -782.78303)	(34.548744 -166.84165 -456.42228)	(143.11208 -166.84165 -1239.2053)
rrw	(3.9722773 -13.320954 12.739888)	(0.012002331 -0.2355339 0.1010956)	(3.9842796 -13.556488 12.840984)
rsw	(-3.3549084 -1.2435416 -1.2495712)	(0.011474427 -0.20831357 0.050961225)	(-3.343434 -1.4518552 -1.19861)
rw	(3.8682819 -8.3113519 -312.4472)	(0.0011479269 -0.038151966 0.31181775)	(3.8694298 -8.3495038 -312.13538)
ut	(-0.20291036 -0.73011049 -20.586593)	(-0.0041036777 -0.020461021 1.2193389)	(-0.20701404 -0.75057151 -19.367254)
wheel-radii	(-0.080410716 -0.076828481 1.2770764)	(-0.00013778659 -0.00062087638 0.0093072457)	(-0.080548502 -0.077449357 1.2863836)

Figure 68: Moments 40m Cornering Radius

Appendix O: Numerical Method Script for ANSYS 22

```
/file/set-tui-version "22.1"

; Fluent Input File

;----------------

; start transcript file [checked]

/file/start-transcript outputfile.txt


; Read mesh file [checked]

/file/read-case Geom_vol.msh.h5


;Set Model [checked]

/define/models/viscous/ke-realizable? y


;Set Boundary Conditions

/define/boundary-conditions/velocity-inlet inlets n n y y n 0 n 0 n n y 5 10

/define/boundary-conditions/pressure-outlet outlets y n 0 n y n n y 5 10 y n n n

/define/boundary-conditions/wall floor y motion-bc-moving n y n n 0 1 0 0 n n 0 n .5

/define/boundary-conditions/fluid domain n n n y -1 n 3.334 n 0 n 0 n 0 n 0 n 0 n 5 n 0 n 1 n 0 none n y n n n

/define/boundary-conditions/wall rlw y motion-bc-moving n n y n n 0 n .5 n 13 .977702 .193 .71029 0 0 1

/define/boundary-conditions/wall rrw y motion-bc-moving n n y n n 0 n .5 n 13 .977702 .193 .71029 0 0 1

/define/boundary-conditions/wall flw y motion-bc-moving n n y n n 0 n .5 n 13 -.532298 .193 -.71503 0 0 1

/define/boundary-conditions/wall frw y motion-bc-moving n n y n n 0 n .5 n 13 -.532298 .193 -.71503 0 0 1


;Set Solver

/solve/set/warped-face-gradient-correction enable? y y

/solve/set/high-order-term-relaxation enable? y

/solve/set/number-of-iterations 1500
```

```
/solve/set/p-v-coupling 24
/solve/set/discretization-scheme/k 1
/solve/set/discretization-scheme/epsilon 1
/solve/monitors/residual/convergence-criteria .000001 .000001 .000001 .000001 .000001 .000001
/solve/set/pseudo-time-method formulation 0

;Set Reference Values
/report/reference-values/area 1.687
/report/reference-values/length 2.815
/report/reference-values/velocity 16.67
/report/reference-values/zone domain

;Initialise
/solve/initialize/hyb-initialization


; Set the number of time steps and iterations/step
/file/auto-save/data-frequency 150
/solve/iterate 1500


;----------------

; Save Case & Data files
/file/write-case-data Final_Output_File.cas

; end transcript file
/file/stop-transcript
/exit yes
```

Appendix Q: Risk Assessment (taken from project progress)

No	Hazard, Activity, Task or Process	Identified Risks	Initial Risk Level	Proposed Control Measures	Residual Risk Level	Notes, Progress Management & Current Risk Level
1	QUTM and FSAE members Relation/ Communication.	Poor communication with the QUTM team may prohibit: -Project development regarding necessary files for simulations. -Information for the dynamic simulations with its associated mechanical properties. -Possibility of testing. -Alignment of desired outcomes.	MODERATE +	-Attend weekly meetings with the FSAE thesis team to frequently catch up on projects, and with the members and supervisor. (Administrative Control) -Build relations with the QUTM team and communicate via discord for any updates and enquires. (Administrative Control)	LOW +	Within progress there has been frequent interaction with both teams. As well as the admission of files, and information regarding the EV4. -There needs to be greater efforts with QUTM regarding projected outcomes. (Administrative Control) MODERATE -
2	HPC Unavail-ability.	Timeliness of stages and completion of project may be affected by potential unavailability of the HPC caused by: -Large queues with heavy simulations. -Maintenance. -HPC account. -HPC being in a coded format through PUTTY.	HIGH	-Ahmed body simulations will be dedicated on personal/standard computers. (Administrative Control) -All simulations will be initialised through personal/standard computers to reduce dependency on the HPC and time wastage. (Administrative Control) The HPC will only be utilised if personal/standards computer are not capable of sufficient quality and refinement. (Administrative Control)	MODERATE -	Progress has obtained a HPC account and usability. Also has revaluated the risk associated with queues and maintenance being less consequential than anticipated. However, the dependency on the HPC is becoming increasingly apparent with extensive refinement and computational time needed for the Ahmed body simulations. -Thus, the project must prioritise its timeline and must not leave HPC

				HPC Heat account will be requested ASAP. (Elimination) The HPC will be tested to confirm ability/usability. (Elimination)		simulations too late. (Administrative Control) MODERATE
3	Simulation Time.	The computational time required by the simulations may impede timeliness of stages, quality, and outcomes.	HIGH	The timeline must be followed closely. (Administrative Control) Complex simulations must utilise the HPC to reduce computational time. (Elimination)	MODERATE -	Progress has fallen short with the timeline projected in the proposal. Simulations are more time consuming and difficult than expected. -A new outlined timeline still allows enough time but must be followed which requires work over the holidays. (Administrative Control) MODERATE
4	Simulation Quality.	An inaccurate simulation will render somewhat useless for the QUTM team.	HIGH	-The project methodology must be followed closely. (Administrative Control) Complex simulations must utilise the HPC to reduce computational time. (Elimination)	Low	Simulations are more time consuming and difficult than expected. -The new timeline and the proposed methodology will facilitate a quality simulation. (Administrative Control)
5	Impractical Simulation.	Small discrepancy may misguide and misdirect the team's efforts and evaluation of cornering performance.	MODERATE +	-A dynamic simulation will allow greater analysis for the FSAE-A with more practicality and less discrepancy. (Elimination) -Report any inaccuracies, limitations, and variables not considered within the simulation. (Engineering Control)	MODERATE -	No explicit progress. NA. MODERATE -

6	Dynamic Simulations	Unable to incorporate practical cornering conditions for a dynamic simulation. Unable to simulate the complex simulation. Unable to validate.	MODERATE	-Appropriate sufficient cornering conditions and mechanical properties with the QUTM team. (Administrative Control) -Verification within 'true cornering' can infer high levels of confidence. (Substitution) -Report limitations (Engineering Control)	MODERATE -	No explicit progress. NA. MODERATE -
7	On-track Testing	Requires QUTM members admission and facilitation. Damage to the EV4. Damage to bystanders/involved members.	Low+	-Gain appropriate relation and communication with the QUTM team. (Administrative Control) -Appropriate driver and set up with the existing QUTM members. (Elimination) -Testing devices must be secured to the vehicle. (Elimination) -PPE equipment eg. Shoes, race suit & helmet gloves and gloves for the driver. Safety glasses, long tight-fitting clothing, and shoes for the surrounding members. Along with a designated fire extinguisher and hydration for the members especially the driver. Water, Shelter, etc. (PPE)	Negligible	Is considered an extension to the project and is unlikely to occur. But if all mechanical properties, and practical conditions are established then it will.

8	Sickness/Illness	Any effecting progress such as sickness or illness or accidents.	LOW	Highlight and discuss with supervisor, and all stakeholders including the QUTM team. Possible extension/repurposed/overtaken. (Administrative Control)	Negligible	NA

Table 7: Risk Assessment

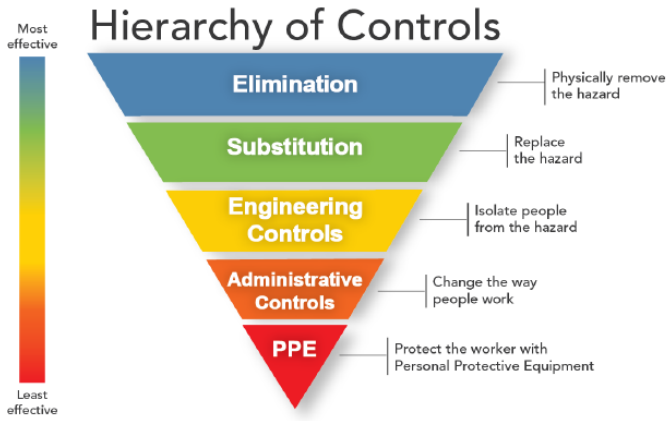

Likelihood	Consequences: Insignificant	Minor	Moderate	Major	Catastrophic
Almost Certain - Expected in most circumstances	Low +	Moderate +	High	Very High	Extreme
Likely - Will probably occur in most circumstances	Low -	Moderate -	Moderate +	High	Very High
Possible - Might occur at some time	Negligible	Low -	Moderate -	Moderate +	High
Unlikely - Could occur at some time	Negligible	Low -	Low +	Moderate -	Moderate +
Rare - May occur only in exceptional circumstances	Negligible	Negligible	Negligible	Low -	Low +

Consequences	How severely could it hurt someone/cause damage?
Catastrophic	Death or large number of serious injuries, environmental disaster, huge cost
Major	Serious injury, extensive injuries, severe environmental damage, major cost
Moderate	Medical treatment required, contained environmental impact, high cost
Minor	First aid treatment required, some environmental and/or financial impact
Insignificant	No injuries, low financial/environmental impact

Risk score	What should I do?
Extreme	Immediate action required
Very High	Senior management attention required
High	Action plan required, senior management attention needed
Moderate	Specific monitoring or procedures required, management responsibility must be specified
Low	Manage through routine procedures
Negligible	Accept the risk

Figure 69: Risk Rating and Hierarchy Control

Appendix U: Risk Assessment

Engineering Code of Ethics	Actions/Notes
1.1, 1.2 , 3.3 , 4.1	-Progress has been truthfully communicated amongst all stakeholders to accurately display project development. This is imperative to allow appropriate alignment and facilitation from the stakeholders.
1.1 , 1.2 , 2.2 , 2.3 , 3.3	-Problems/issues have been mentioned to David Holmes, and QUTM aerodynamic members who are considered authoritative and competent sources.
1.3	-Relationships with the stakeholders is imperative towards the project. Thus, all members have been communicated in a respectful, friendly, and courtesy manner.
2.1, 2.2, 2.3, 3.1	-The project methodology will enable high levels of confidence if its iterative stages are conclusively developed upon. -All results have been heavily analysed to concur its quality and level of confidences through verification of cornering airflow with theoretical values. Also, validation of case studies which exhibit high levels of confidence and comparability. -All discrepancies, and limitations have and will continue to be detailed upon. Results have not been presented in a misleading manner or manipulated to exhibit greater quality and progress. -All risks and sustainability concerns have been discussed in detail.
2.2	-It is important to note, that I am studying a mechanical engineering degree. Whilst, this project is based on aerodynamics, I have developed sufficient abilities prior to commencement. It will be expected that I do not have all required abilities, however, the project methodology, QUTM aerodynamic members, and David will greatly build upon my competencies and allow Questions, or enquiries will be conducted through those with high levels of competency namely David Holmes, the aerodynamic members of the QUTM team, and prior project students.
4. Promote sustainability	-All sustainability concerns have been incorporated within the project detailed below.

Table 8: Engineering Code of Ethics